Aus der Klinik für Hals–Nasen–Ohrenheilkunde,
Universitätsklinikum des Saarlandes, Homburg/Saar
Direktor: Prof. Dr. med. Bernhard Schick

On the Fast Detection of Auditory Brainstem Responses: A Novelty Detection Paradigm

Dissertation zur Erlangung des Grades eines
Doktors der Theoretischen Medizin
der Medizinischen Fakultät
der UNIVERSITÄT DES SAARLANDES
2009

vorgelegt von:

Farah I. Corona–Strauss, M.Sc.

geb. am: 14. Dezember 1977 in Mexiko Stadt

Dekan: Prof. Dr. med. Michael D. Menger

Referent:

Korreferent:

Tag der mündlichen Prüfung:

TO MY HUSBAND
&
MY PARENTS

Summary

The evaluation of auditory brainstem responses (ABRs) is accepted as a robust method for the objective detection and quantification of hearing loss in non–cooperative patients. In currently available ABR analysis technologies, a large number of sweeps (individual responses) has to be averaged in order to obtain a meaningful signal morphology due to a poor signal–to–noise ratio. The computation of such large–scale averages makes the evaluation of ABRs time consuming, limiting the applicability of this method crucially.

This thesis proposes a completely new detection paradigm for ABRs by means of a fast ABR single sweep processing. This paradigm is called *the novelty detection paradigm*. Here the ABR evaluation system is adjusted to the spontaneous electroencephalographic activity and correlates of a stimulus locked synchronization at the brainstem level, as indicator of a physiological hearing, are detected as novel instances. The features used in this paradigm are based on the inter–sweep instantaneous phase synchronization as well as energy and entropy relations in the time–frequency domain. Included in the evaluation of this new approach was the test of different broadband stimuli (click and chirp) and different Ag/AgCl electrodes (active and passive). It is concluded that the proposed novelty detection paradigm allows for a much faster detection of ABRs than conventional averaging methods and that the ABR detection can be improved by the chirp stimulation technique.

Apart from this novelty detection paradigm, an independent part of this thesis was dedicated to the optimal frequency specific auditory stimulation as prerequisite for subsequent feature extraction and ABR detection stage. In particular, a new family of notched–noise embedded band limited chirps for the assessment of frequency specific ABRs has been developed and calibrated. The evaluation of these chirps in healthy young adults as well as the analysis of the corresponding ABRs using phase synchronization methods are reported. It is concluded that the assessment of frequency specific ABRs is possible using this new family of chirps which can be employed in the novelty detection paradigm.

Zusammenfassung

Die Evaluierung von auditorisch evozierten Hirnstammpotenzialen (AEHPs) ist ein etabliertes Verfahren zur sicheren objektiven Detektion und Quantifizierung einer Hörstörung bei nicht–kooperativen Patienten. Aufgrund eines sehr schlechten Signal–Rausch–Verhältnisses muss in derzeit verfügbaren Technologien zur AEHP Analyse eine hohe Anzahl von Einzelsweeps, d.h. elektroenzephalografische Antworten auf einzelne Stimulationen, gemittelt werden um eine aussagekräftige Signalmorphologie zu erhalten – insbesondere bei geringen Stimulationsintensitäten. Diese Berechnung von großskaligen Mittelwerten macht die Analyse von AEHPs sehr zeitintensiv und limitiert daher die Anwendbarkeit dieser Methodik deutlich.

In dieser Arbeit wird ein völlig neues Paradigma zur ultra–schnellen Detektion von AEHPs auf der Basis von Einzwelsweeps vorgestellt, welches das *Neuheiten– Detektions–Paradigma* genannt wird. Danach wird das AEHP Analysesystem erstmals an die elektroenzephalografische Spontanaktivität angepasst und Korrelate einer – in Bezug auf den Stimulus – zeitfesten Synchronisation auf Hirnstammniveau als Indikator eines physiologischen Hörens als "Neuheiten" detektiert. Die in diesem Paradigma verwendeten Merkmale basieren auf einer Inter–Sweep Synchronisation der Momentanphase sowie Energie– und Entropierelationen in der Zeit– Frequenzebene. Die Evaluierung dieses neuen Verfahrens umfasste auch einen Test von verschiedenen breitband Stimulationen (Klick und Chirp) sowie verschiedene Ag/AgCl (passive und aktive) Elektroden. Es wird gefolgert, dass der vorgeschlagene neue Zugang eine wesentlich schnellere Detektion von AEHPs als konventionelle Mittelungsmethoden erlaubt und optimal durch die Chirp–Stimulation ergänzt wird. Neben dem Neuheiten–Detektions–Paradigma, wurde sich in dieser Arbeit der optimalen frequenzspezifischen Stimulation als Voraussetzung für die folgende Merkmalsextraktion und AEHP Detektion gewidmet. Insbesondere wurde eine neue Serie von in einem Kerbrauschen eingebetteten, bandlimitierten Chirps für die frequenzspezifische AEHP Analyse entwickelt und kalibriert. Über die Evaluierung dieser Chirps bei gesunden jungen Erwachsenen sowie über deren Phasenstabilitätsanalyse wird in dieser Arbeit berichtet. Es wird gefolgert, dass die frequenzspezifische Bewertung von AEHPs durch diese neue Serie von Chirps, welche sich in das Neuheiten– Detektions–Paradigma integrieren lässt, möglich ist.

Contents

Notation

$\mathbb{N}$	the set of natural numbers, $\mathbb{N}_0 = \mathbb{N} \cup \{0\}$
$\mathbb{Z}$	the set of integers
$\mathbb{R}$	the set of real numbers
$\mathbb{R}_{>0}$, $\mathbb{R}_{\geq 0}$	$\mathbb{R}_{>0} =]0, \infty[$, $\mathbb{R}_{\geq 0} = [0, \infty[$
$\mathcal{C}^k(\mathbb{R})$	the space of k times continuously differentiable functions on $\mathbb{R}$
$L^2(\mathbb{R})$	the Hilbert space of all square integrable functions
ℓ^2	the Hilbert space of all square summable sequences
$\langle \cdot, \cdot \rangle_{\mathcal{H}}$, $\|\cdot\|_{\mathcal{H}}$	inner product and norm on a Hilbert space $\mathcal{H}$
$\|\cdot\|_2$	Euclidean norm
$K(\cdot, \cdot)$	reproducing kernel
$*$	convolution product
$\times$	the Cartesian product
$\oplus$	direct sum
span	finite linear combinations
$\mathcal{H}_K$	reproducing kernel Hilbert space

Chapter 1

Introduction

1.1 Hearing Loss in Newborns

Congenital hearing loss is a common and important health problem and one of the most common neurosensory handicaps in newborns and children (Yoshinaga-Itano, 1999; de Aledo Linos, 2001; Sivalal, 2005). Therapies for newborns with bilateral hearing loss are important during their first 24 weeks of life as otherwise a serious delay in speech and intellectual development has to be expected, see Yoshinaga-Itano (1999). It is difficult, if not impossible to acquire fundamental language skills, social skills, and particular cognitive skills for this patient group. Thus there is no foundation for later schooling and success in the society. The consequences of being deaf–mute are special schools and care, social isolation, and no exploitation of potential skills. Thus there are serious medical and economical consequences for the entire society due to this problem, see Yoshinaga-Itano (1999); de Aledo Linos (2001).

According to Sivalal (2005) the prevalence of congenital permanent childhood hearing impairment (PCHI) differs from country to country. This irregularity is partly due to differences in study population, criteria for impairment and the tests that were used in the study. The prevalence of PCHI has been estimated to be, e.g., 1.1 to 1.5 for every 1000 live births in Estonia, 2 to 4 in 1000 in the U.S.A, and 1 in 900 in the U.K.. The prevalence of sensorineural hearing loss also varies with race, birth weight, and other risk factors. In 30% of the cases, these children had other neuro–developmental conditions, most frequently mental retardation. The prevalence of hearing loss in high risk newborns is 10 to 20 times higher than in normal newborns. PCHI has been said to

be more prevalent than commonly screened medical conditions such as phenylketonuria, hemoglobinopathies and congenital hypothyroidism, see Sivalal (2005).

1.2   Organization of NHS and Hearing Screening Techniques

Different newborn hearing screening (NHS) programs to detect hearing loss as early as possible have been established so far, see Helfand et al. (2001); Delb (2002, 2003). The technical methods used in these programs include otoacoustic emissions (OAEs), and auditory evoked responses (ABRs).

Other methods such as the middle latency responses (MLRs), and auditory late responses (ALRs) can not be used in the NHS programs because they are not reliable in young infants, i.e., the MLRs can be or can not be present in healthy babies (Stapells, 2000; Stapells et al., 1988), on the other hand ALRs can be susceptible to changes under sleeping conditions (Stapells, 2000) or be influenced by diverse endogenous factors, such as attention (Low et al., 2007).

Next, short descriptions of the already mentioned methods used for hearing screening purposes are given.

1.2.1   Otoacoustic Emissions

The OAEs are sound responses that are emitted from the ear. There are two types of OAEs screening techniques, transient evoked otoacoustic emissions (TEOAEs) and distortion product otoacoustic emissions (DPOAE) (Delb, 2003; Plinkert and Delb, 2001; Delb et al., 1999; Helfand et al., 2001; Delb et al., 2004). TEOAEs are generated in response to clicks, see an example of a click in Fig. 1.3, while DPOAEs are responses to tones. Both stimuli are presented to the patient via lightweight ear canal probes. A microphone picks up the signal, and multiple responses are averaged to get a reproducible waveform. This test can be carried out at the bedside and a "pass response" or "fail response" is recorded. TEOAE measurements are more commonly used for infant screening.

The absence of TEOAE indicates that the inner ear is not responding appropriately to sound. Thus, TEOAEs can be used for a hearing check but they do not allow for a quantification, degree or type of the hearing loss (Stapells, 2000). Moreover, a large proportion of healthy children are classified as hearing impaired, i.e., the specificity of this method is rather low, see Delb (2003).

1.2.2 Auditory Evoked Responses

The ABR is an electrophysiological response in the electroencephalogram (EEG) generated at the level of the brainstem in response to auditory signals such as clicks, chirps, or bursts of tones, see an example of an ABR waveform in Fig. 1.1, and an example of a click and a chirp in Fig. 1.3. ABRs are also named brainstem auditory evoked responses (BAERs), and brainstem auditory evoked potentials (BAEPs) (Hall, 1992). ABRs are generated by the delivery of stimuli via earphones or an inserted ear probe; scalp electrodes are used to obtain the signals. The characteristic features of the ABRs are amplitude and latency of their wave components. Latency is a term used to describe the time at which an evoked response wave component occurs after a stimulus (Hall, 1992); in the case of ABRs the dominant wave is the so–called wave V component (its latency when using click auditory stimuli is in the 5.0-10.0 msec post– stimulus region). The amplitude and latency of an ABR are related to the intensity and the characteristics of the auditory stimulus that is employed.

Detection of wave V in ABR measurements is a robust method for the objective diagnosis and quantification of hearing loss in children (Wicke et al., 1978; Woodworth et al., 1983; Mason and Adams, 1984; Peters, 1986; Shangkai and Loew, 1986; Delb, 2003). This method has a higher specificity as the TEOAE measurement and provides information about the integrity of the auditory pathways from the auditory nerve until the level of the brainstem (Stapells, 2000), see Fig. 1.1. Click evoked–ABRs, which are usually used in NHS programs, can be used for the detection of the hearing threshold (HT), i.e., the quantification of the hearing loss, but one disadvantage is that they can not estimate hearing losses in particular frequency regions (low, middle or high frequencies) (Stapells, 1994).

Also, due to a poor signal–to–noise ratio, 2000 to 4000 sweeps (individual responses) have to be averaged to obtain a meaningful, visually noticeable signal at a particular
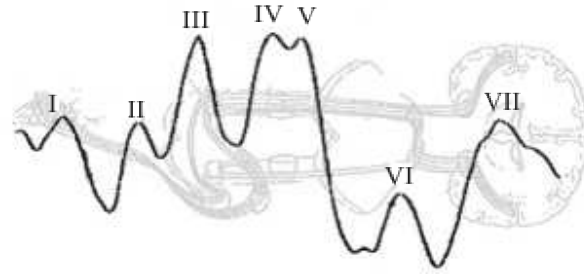
Figure 1.1: Example of an ABR waveform. The components of the ABR are numbered with Roman numerals. Each wave corresponds to a specific structure along the auditory pathway. Some of the generators of these waves are still under discussion. Wave (I): VIII-auditory nerve, (II): cochlear nuclei, (III): superior olivary complex, (IV): nucleus of the lateral lemniscus, (V): inferior colliculus, (VI and VII): medial geniculate body of thalamus. For more detailed information we refer to Hall (1992). Picture taken and modified from Hall (1992)

.

stimulation level (the exact number depends on the number of artifacts produced). As such large–scale averaged signals are used in the conventional visual analysis, they are also commonly used in computational scheme although — for a machine – other data representations might be more appropriate (Strauss et al., 2004b).

Using the currently available devices this takes approx. 2 to 4 minutes to get the result for one stimulation level, e.g., see Meier et al. (2004) where it was not possible to obtain a reliable response in less than even 4 to 5 minutes. This measurement time requires sometimes the state of spontaneous sleep, strong sedation, or narcosis of the newborns. NHS programs are therefore commonly conducted as multiple stage procedures, see in Fig. 1.2 the implementation of a NHS program in the state of Saarland, Germany.

Evidently, follow ups are often missed in such schemes, hence losing the effectiveness of the program. This multiple stage implementation is necessary because of the technical problems described before. The ABR measurement can just be applied at the last screening stage due to the long duration measurements. In other words, the idea is to filter as many as possible newborns by TEOAE measurements but due to a low specificity, many newborns with a physiological hearing are transferred to subsequent screening stages and this produces unnecessary cost due to the follow up.

So far, many methods have been proposed for an automatic recognition of ABRs with
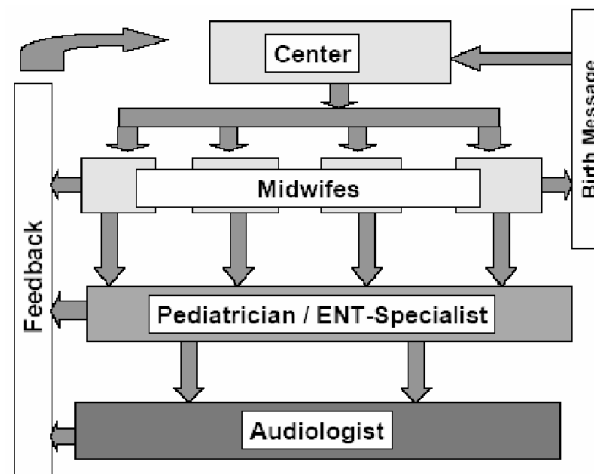
Figure 1.2: Organization of a 3–stage universal NHS program implemented in the state of Saarland, Germany.

various success rates (Wicke et al., 1978; Woodworth et al., 1983; Mason and Adams, 1984; Peters, 1986; Shangkai and Loew, 1986; Madhavan et al., 1986; Delgado et al., 1988; Dobie and Wilson, 1989; Özdamar and Alpsan, 1992; Alpsan et al., 1994; Chen et al., 1996; Sanchez et al., 1995; Popescu et al., 1999; Vannier et al., 2002; Gentiletti-Faenze et al., 2003; Strauss et al., 2004b). These methods are essentially based on traditional statistical pattern recognition techniques for classification of the ABRs. Generally, signal characteristics pertaining to different conditions are derived and then used for the computational recognition. Syntactic methods have also been used for the classification of ABRs (Madhavan et al., 1986).

Developing intelligent recognition systems using statistical or syntactic procedures faces great difficulties, since signal characteristics or rules are not readily extractible. Although medical experts can interpret these signals, they can not identify the rules completely, see Alpsan et al. (1994); Acir et al. (2006). Artificial neural networks are also used for classification of ABRs, e.g., Özdamar and Alpsan (1992). The estimation of the HT using ABRs involves the determination of the lowest stimulus intensity at which a sound evoked wave can be observed in the recording. Therefore an important step in automated threshold determination is to make a decision as to whether a sound evoked response is present in the waveform. Each ABR patterns recorded at a given intensity must be labeled into a "with response" and "without response" class on the basis of presence or absence of sound evoked peaks in the waveforms.

The primarily difficulty in this classification task is the differentiation of actual responses from the peaks that are due to EMG activity and noise. In Chen et al. (1996) was reported a clinical evaluation of the widely used detection method "ALGO", developed by Peters (1986), with a sensitivity of 93%, a specificity of 78% and an accuracy of 83%. In Özdamar and Alpsan (1992) was reported an accuracy of about 76% for ABRs classification by using backpropagation multilayer perceptron classifier for the purpose of threshold determination. In Vannier et al. (2002) was reported a rather good sensitivity (91%), specificity (92%) and accuracy (91%) using an automatic ABR statistical recognition.

A high accuracy of 97% was reported by Sanchez et al. (1995) using a vector of several attributes estimated from the ABRs. Due to different measurement techniques, data acquisition procedures, and processing techniques it is difficult to objectively compare the results of the research cited above.

However, all of the above cited methods are based on large–scale averaging procedures for the final analysis and require sometimes narcosis, sedation, or the state of spontaneous sleep of the newborn to obtain the data. It is the major objective of this work to avoid time–domain averaging procedures, and instead use single sweep analysis in order to implement a very fast detection of the hearing loss and HT, respectively.

1.2.3   Frequency Specific Threshold Detection

In general applications, i.e., NHS programs, the already mentioned hearing screening methods give results related to a general HT, and when a more detailed frequency specific determination of a HT is required, different approaches are used instead, e.g., pure tone–evoked ABRs, auditory steady state responses (ASSRs) (Luts and Wouters, 2004) (such as the amplitude modulation following responses (AMFRs) (Pethe et al., 2002)), stacked ABR (Don et al., 1997, 2005), and notched–noise brainstem evoked responses (Stürzebecher et al., 1994).

The pure tone–evoked ABRs are responses elicited by sinusoidal burst stimulations at fixed frequencies, commonly the standard frequencies used in subjective audiograms. The subsequent processing steps are based on averaging techniques as for normal ABRs.

The ASSRs are enhanced by modulated sinusoidal waves or by broadband stimuli, such as clicks or chirps (Elberling et al., 2007; Burkard et al., 2006) at high repetition rates,

and the analysis is performed in the frequency domain. Although ASSRs might be very promising for the objective adjustment of hearing aids, it can be very time consuming to obtain these signals, see Pethe et al. (2002).

The stacked ABR method has been used for the detection of small acoustic tumors, and seems to be a promising approach for frequency specific HT determinations. This technique combines click–evoked ABRs together with a high–pass masking noise at different cut–off frequencies. The waves V are then determined for different frequency bands by subtraction of the average response obtained without masking condition from the subsequent average responses using masking noise with decreasing cut–off frequencies, see Don et al. (1997, 2005) for details.

In the notched–noise evoked responses the ABRs are generated by a combination of clicks or bursts of pure tones together with notched–noise centered at different frequencies.

In summary, the pure tone–evoked ABRs, stacked ABR, and notched–noise evoked responses depend on the detection of a time domain waveform, like the regular ABR detection method, which means that they use time consuming averaging techniques in the range of thousands of sweeps in order to have an identifiable wave V. Therefore a fast detection of frequency specific ABRs would also be of great relevance in all these applications, and not only for click–evoked ABRs, where the interest is a general HT determination.

1.3   Chirp Stimulus

In the past it was commonly believed that ABRs were elicited by the onset or offset of a stimulus, and therefore clicks were preferred because of their abrupt onset and wide spectral content, e.g., see Hall (1992); Kodera et al. (1977) – similar to the idea of a Dirac distribution activating all the Eigenvalues of a continuous linear time invariant system.

From cochlear mechanics is known that the cochlea is tonotopically organized (de Boer, 1980). This means that low frequency components of a traveling wave take a longer time to reach their sensation locus (apex) than the high frequency components (base), see Fig. 1.3 for a schematic diagram of the cochlea. Gorga et al. (1988); Neely et al.

(1988) reported wave V latency curves and showed that the latency and amplitude of the wave V were related to the intensity and the frequency of the stimulus. Later, Dau et al. (2000a) created a chirp stimulus to evoke ABRs that was designed to compensate the temporal dispersion of the basilar membrane (BM) (delaying high frequencies components from the low frequencies) by using the linear cochlear model of de Boer (de Boer, 1980) and the cochlear frequency–position functions based on experimental data obtained by Greenwood Greenwood (1990), see Fig. 1.3 for an example of a chirp stimulus.

In Fobel and Dau (2004) the authors designed a variety of chirps using different data sources, such as OEAs data, and ABR wave V–latency plots. The chirps in general evoked larger responses than click stimulations. The chirps which showed the best responses, specially for low stimulation levels, were calculated using the wave V latency curves, which are sensitive to intensity. This latency curves represent a better approximation from the point of view of cochlear mechanics.

As previously stated, the use of chirps had not only been limited to ABRs, but also to ASSRs, for details see Elberling et al. (2007). Thus, due to its promising features and variety of possible applications, the chirps have become more popular over the last years. Part of the present work is dedicated to the use of chirps for: (1) collection of brainstem responses, and their respective comparison against click–evoked responses; and (2) the development of a family of notched–noise embedded band–limited chirps for the assessment of frequency specific ABRs.

1.4   The Novelty Detection Paradigm

Single Sweep Analysis: As mentioned before, time consuming averaging procedures are used for the evaluation of ABRs, which make their measurement unsuitable in early screening stages of universal NHS programs. The authors in Strauss et al. (2004b) suggested a hybrid signal processing scheme for ABR single sweeps which allowed the detection of wave V in just a fraction (10%) of the measurement time of conventional approaches at 30 dB HL stimulus, i.e., 12 sec. and 24 sec. instead of 2 min and 4 min, respectively. See Fig. 1.4 for an example of ABR single sweeps representation.

Moreover, as in–situ measurements by Stevens et al. (2004) showed, there is no available device at the moment – although there are different manufacturers' instructions – which
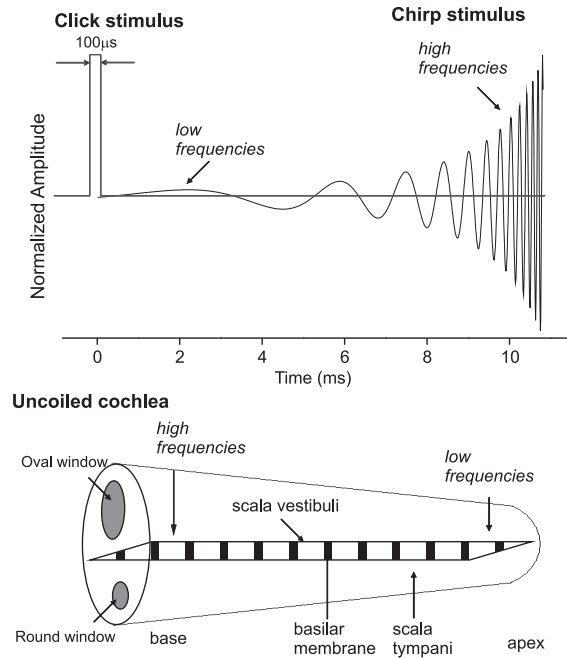
Figure 1.3: (Top) Broadband Stimuli: click stimulus with a duration of 100 μs, represented with a dark gray line, and chirp stimulus, with rising frequency, represented with a black line. Note that for the chirp, the low frequencies are delayed from the high frequencies, and its amplitude envelope assures a flat amplitude spectrum. (Bottom) Schematic of the cochlea. Note the tonotopic organization: the sensation loci for high frequencies are in the area of the base and for low frequencies in the area of the apex.

allows the detection of a hearing loss below 45 dB HL. At 30 dB HL it is of course more difficult than for larger stimulation levels as the responses are much weaker. Note that the combination of kernel machines and wavelet methods has recently also been adopted by other groups (Acir et al., 2006) but for large–scale averaged responses which are too time consuming for the purpose of this work.

Consequently, with such a fast hybrid signal processing procedure the HT could be detected at low stimulation levels at the first screening stage. This would thus also allow the quantification of hearing loss when considering an increasing stimulation level. In other words, there would be not just the information "deaf" or "not deaf" but also a specification of the hearing loss. The procedure in Strauss et al. (2004b) is based on the design of paraunitary filter banks for the implementation of wavelet frame decomposition which are tailor–made for kernel learning machines merged with a
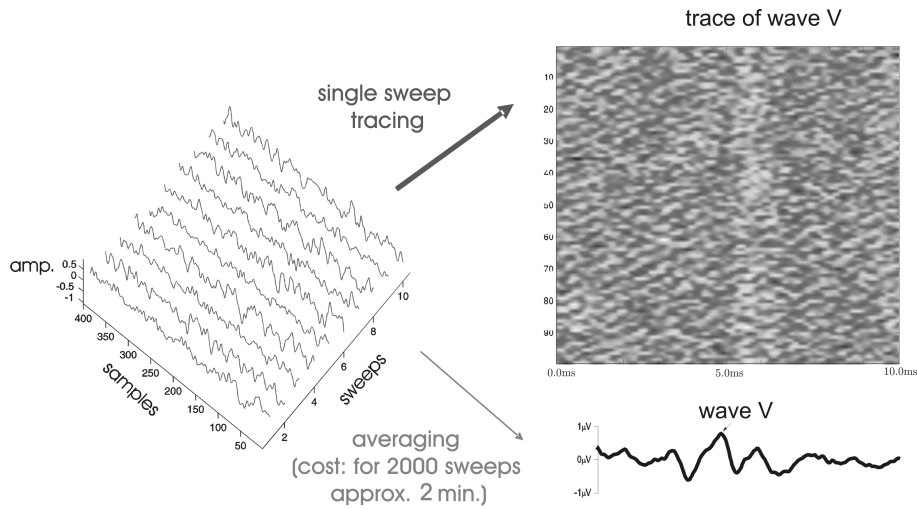
Figure 1.4: Left: single sweeps (individual responses); Right (bottom): the averaged signal (approx. 2000 sweeps) commonly used in the ABR analysis; Right (top): single sweeps in matrix representation (The normalized amplitude is coded in gray colors ranging from black to white, which represent small and large amplitudes, respectively), here the trace of wave V is clearly noticeable. In this single sweep matrix representation, amplitude fluctuations and latency jitters are also discernible, which is information that is lost in the averaged response.

inner sweep dissimilarity analysis. In other words, shift–invariant frame transforms are designed to optimize (in the sense of statistical learning theory) the feature extraction in ABRs for a subsequent detection by kernel learning machines, see Fig. 1.5.

The Novelty Detection: In Strauss et al. (2004b) was showed that a single sweep analysis of ABRs can be used for the detection of wave V and thus for a detection of the hearing loss. However due to the limited data substrate used this can just be seen as the proof of the feasibility of the approach (Strauss et al., 2004b). Also the time of the learning phase of the kernel based scheme could be reduced or even avoided when using the phase synchronization measures discussed in the next section.

However, the most important drawback is that there is still no way to include the individual measurement setup in the computational analysis as discussed in Strauss et al. (2004b). Therefore it is the objective of this work to realize the paradigm change to a measurement setup adapting neural signal processing of ABRs. The basic idea is to design a computational recognition scheme that is adjusted to the individual measurement condition using the spontaneous EEG activity. In the next step, auditory
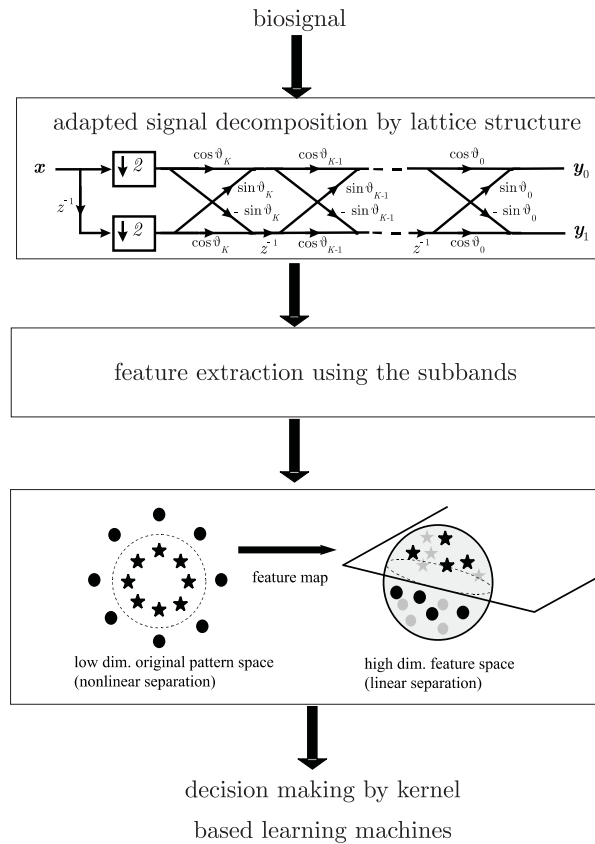
Figure 1.5: The principle of a hybrid wavelet–kernel learning machine: adaptive feature extraction and inclusion of prior knowledge (stage 1 and 2) and decision making by kernel machines (stage 3).

stimulations at larger stimulation levels are applied, e.g., at 30, 40, and 50 dB SPL. If there is a stimulus locked reaction of the brainstem to the stimulus – thus a physiological hearing, a regular and consistent event must be present in the respective time interval. The detection of such a regular, consisted, stimulus locked event is very challenging due to the single sweep processing and represents the major scientific challenge of this work.

This new paradigm may provide the basis for a radical innovation in the objective hearing examination of newborns. Two different approaches seem to be promising at the moment to implement such an adaptive procedure computationally.

Several statistical, kernel, and neural network based novelty detection approaches have been introduced in recent years, see Markou and Singh (2003a,b) and references therein for an excellent review. Under all these schemes, kernel based novelty detectors are

electroencephalographic data

**Transform Analysis
(feature extraction)**

representation by abstract features

novel events
(presents of abstract
ABR correlates)

sphere constructed from the
spontaneous activity in the
calibration phase (known events)
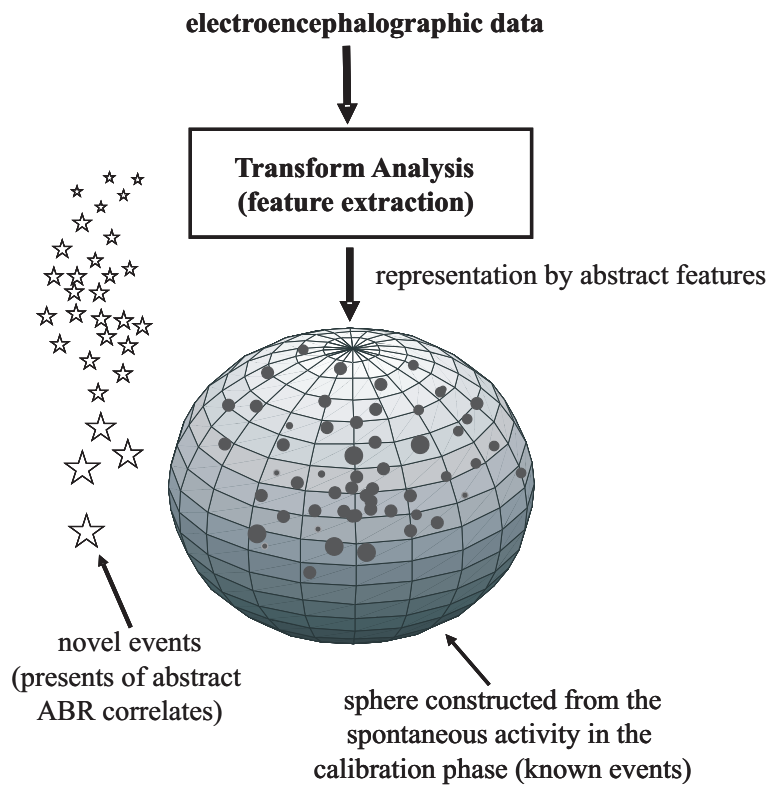
Figure 1.6: Sketch of the novelty detection idea: the system is adjusted to segments of the spontaneous activity (no stimulation condition) and a physiological neural brainstem processing of stimulations above the hearing level is detected as novel event.

particularly appealing since they adjust their capacity to the data automatically and involve just the solution of convex, globally solvable optimization problem for their learning (Tax and Duin, 1999).

Kernel based novelty detection machines construct a sphere around the data represented in the feature space. This is the learning task of these machines. After that, new data which is outside of this constructed sphere is detected as novel instance, see Fig. 1.6. Here a tradeoff has to be made between the generalization performance of the machines and their ability to detected events that are abnormal and do not belong to the learned class. In other words, not every slight difference in data which does not belong to the training set has to be detected as novel instance but at the same time abnormal events which do not belong to the learned class have to be detected.

In the new paradigm introduced before, the spontaneous activity of the EEG could be the training data for the hybrid novelty detection machine. This would allow the

inclusion of the individual measurement conditions, e.g., the electrodes configuration.

If now a stimulus at a particular stimulation level above the HT of the subject is applied, there is a novel, regular, and stimulus locked event present in the EEG which can be detected by these machines. Here the optimal feature extraction remains the most challenging part.

1.5 Phase Space Transforms: Synchronization Stability Measures

Recently, time–scale coherence measures based on the complex wavelet transform have been introduced, which take the non–stationary nature of evoked potentials into account in contrast to conventional coherence based on the frequency information alone, see Lachaux et al. (1999); Bruns (2004) for an overview and comparison of the Hilbert and windowed Fourier transform. This wavelet coherence increases with the correlation of the envelopes between two signals as well as if their phases show smaller variations in time (Lachaux et al., 1999).

In contrast to the analysis of averaged potentials, the amplitude information of single sweep event–related potentials, i.e., the response to individual events, turned out to be fragile in some cases (Kolev and Yordanova, 1997). Large amplitude fluctuations can easily be introduced by slight accidental changes in measurement setup over time. Since the signals exhibit a high degree of variance from one sweep to another, even robust amplitude independent synchronization measures such as the time–scale entropy (Strauss et al., 2004a) can hardly be applied to assess their synchronization stability.

To be independent from amplitude fluctuations one can focus on the wavelet phase coherence exclusively (Lachaux et al., 1999). The wavelet phase coherence defined in Lachaux et al. (1999) is mainly applied to measure the degree of phase locking of two signals in time, e.g., obtained from two different sites.

Recently, Strauss et al. (2005, 2008) have shown that this measure can be used for the assessment of the phase synchronization stability as large–scale reflections in auditory late evoked response single sweep sequences. Such an idea could also be applied for the detection of a stimulus locked activity in ABRs. For the spontaneous activity, we have no regular synchronization and thus no time locked responses in the EEG when
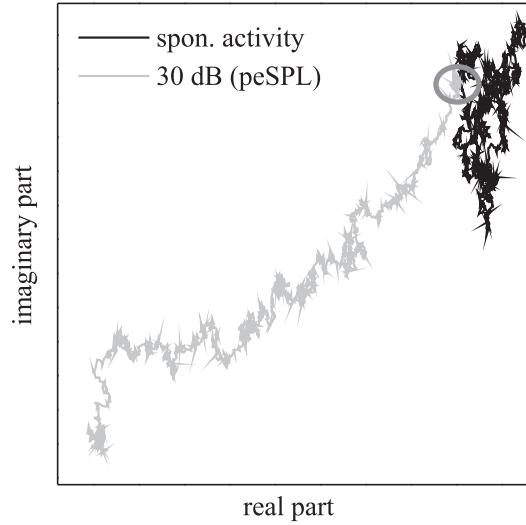
Figure 1.7: The synchronization stability in the complex plane for time intervals of the spontaneous activity (0 dB SPL), shown in gray color, and for auditory evoked response single sweep sequences at 30 dB SPL, shown in black color (the synchronization stability is proportional to the absolut vectorial length of the individual traces). The same number of sweeps was used in both cases. It is noticeable that there is no synchronization for 0 dB SPL but synchronized activity for 30 dB SPL.

considering consistent time intervals. For a stimulation above the hearing level, there is supposed to be a regular synchronization that is time locked with the stimulus. Consequently, there should be a significant increase in the phase synchronization stability as first experiments confirmed, see Fig. 1.7.

Such phase synchronization measures could help to complement supervised kernel learning procedures and thus speed up the scheme significantly. However, this novel technique has also to be modified, improved, and adjusted for ABR detection.

1.6   Contribution of this Work

The main purpose of this work was to introduce a new novelty detection paradigm for the fast detection of ABR single sweeps using abstract phase synchronization measures and machine learning techniques. Moreover, this work was focussed on the evaluation of the best measurement setup, electrodes, and stimulus combination in order to improve the detection and generation of ABRs.

As previously stated, the improved detection of ABRs according to this paradigm started with the data acquisition. For this purpose an acquisition setup was specifically designed in order to collect ABR single sweeps.

Later, the work was focused on developing different types of auditory stimuli to evoke the ABRs. As it has been lately reported in literature that ABRs evoked by optimized chirp signals seem to be promising as the applied rising frequency chirp signal might produce synchronous discharges of VIIIth nerve fibers along the human cochlear partition. It was shown that this may lead to a significant increase of the amplitude of the evoked signals, see Dau et al. (2000b); Wegner and Dau (2002). The previously stated implies that chirps might speed up the application of the proposed detection algorithms. Therefore such optimized chirp signals were also included in this work for the generation of ABR data, and the collected responses were evaluated and compared against a commonly accepted broadband stimuli, i.e., click stimulations.

For the first time, the evaluation of passive and active Ag/AgCl electrodes was done in order to improve the acquisition of the electroencephalographic activity. Recently, active electrodes have been suggested to be easier to attached than commonly used passive electrodes (which sometimes require a laborious skin preparation procedure); to have automatic impedance adjustment due to their pre-polarization and pre-amplification stage, and therefore also lead to an improvement in the compensation for artifacts related to movements.

Subsequently, the goal was to develop a new detection paradigm for ABRs by means of a fast ABR single sweep processing. This *novelty detection paradigm*, as previously stated, adjusted itself to the spontaneous EEG activity and correlates of a stimulus locked synchronization at the brainstem level, as indicator of a physiological hearing, were detected as novel instances. The features used in this paradigm were based on the inter–sweep instantaneous phase synchronization as well as energy and entropy relations in the time–frequency domain.

On the other hand, taking into account the state of the art related to methods such as the notched–noise evoked responses, it was an interesting issue to analyze whether we could exploit a combined approach using band limited chirp stimuli together with notched–filtered noise. Therefore another part of this thesis was dedicated to the development of a family of notched–noise embedded band limited chirps for the assessment of frequency specific ABRs, which had not been used in this configuration before. The

results of the evaluation of these chirps in healthy young adults, and their analysis by using phase synchronization measures was also reported.

Organization of the Work: The information is organized as follows: In the Chapter 2 is explained the measurement setup, the data acquisition procedures, the generation methods of the different auditory stimuli, as well as their calibration. Also here are presented all the necessary formalisms for the novelty detection algorithm and feature extraction calculation, Gabor frame operators and continuous wavelet transform as well as learning machines. In Chapter 3 we show the results of the approach. This includes the already mentioned comparison of different stimuli and electrodes, the results of the novelty detection paradigm, phase synchronization measures extracted with different time–frequency transformations, and the results of the notched–noise embedded frequency specific chirps. In Chapter 4 we present a detailed discussion of the reported results, as well as future work that can still be done. The conclusions are finally given in Chapter 5.

Chapter 2

Material and Methods

In this chapter is given a description of the procedures used to generate different types of auditory stimuli, their calibration method, the measurement setup and experimental procedures used in order to collect auditory brainstem responses.

Also a more detailed explanation of the methods used in the post-processing stage and novelty detection paradigm, such as time–frequency transformations, synchronization measures, and novelty detection machines are given.

As mentioned in the Sec. 1.6, two different studies for data collection were performed. In order to make a clear separation of the two studies used along the entire work, the auditory stimulation protocols and processing sections are distinguished by number, Study 1 and Study 2. The Study 1 was focussed on the comparison between chirp–evoked ABRs and click–evoked ABRs using two different types of electrodes (passive and active), and the Study 2 was performed to evaluate a series of notched–noise embedded frequency specific chirps to asses frequency specific auditory brainstem responses.

2.1 Stimuli

2.1.1 Study 1: ABR–Chirps and Clicks

ABR–chirps: Based on the results reported in Fobel and Dau (2004), the chirps which yielded in the largest evoked responses (in Fobel and Dau (2004) referred as

A-chirps) were calculated. The procedure is following explained. From the equation which represents the ABR wave V latency as reported by Neely et al. (1988):

$$\tau_{\mathrm{BM}}(f) = a + bc^{-i}f^{-d} \tag{2.1.1}$$

with $a = 5.0$ ms, $b = 12.9$ ms, $c = 5.0$, $d = 0.413$, and with i representing the stimulus intensity (in dB SPL divided by 100) and f representing the stimulus frequency divided by 1 kHz, the mechanical component of the latency of wave V was considered as the second term of equation (2.1.1), while the first term was consider as neural component and therefore, independent from frequency and intensity (Neely et al., 1988). The final latency–frequency function resulted in: $\tau_{\mathrm{BM}}(f) = bc^{-i}f^{-d}$.

The variable τ_{BM} was considered to represent the propagation time (Fobel and Dau, 2004), and therefore the inverse function of τ_{BM} was calculated, that is $\tau_{\mathrm{BM}}^{-1}(f) = f_a(t)$, where $t = \frac{1}{f}$.

Next, the chirp was given by

$$S(i, t) = A(i, t)\sin(\phi(i, t) - \phi_o), \tag{2.1.2}$$

with the amplitude factor

$$A(i, t) = \sqrt{\frac{df_a(t)}{dt}} = \sqrt{\frac{(bc^{-i})^{1/d}}{d[t_o(i) - t]^{1/d+1}}} \tag{2.1.3}$$

and the instantaneous phase

$$\phi(i, t) = 2\pi \int_0^t f_a(t)dt = \frac{2\pi(bc^{-i})^{1/d}}{\nu}\left[\frac{1}{(t_o(i) - t)^\nu} - \frac{1}{t_o(i)^\nu}\right] \tag{2.1.4}$$

with $\nu = d^{-1} - 1$ and $t_o = \tau_{\mathrm{BM}}$ (100 Hz). We refer to Fobel and Dau (2004) for further details.

Three different chirps were computed, using Eq. (2.1.2), (2.1.3), and (2.1.4), for the intensity levels of 40, 30 and 20 dB sound pressure level (SPL). The frequency range for all the chirps was from 0.1 to 10 kHz. The resulting durations were 7.84, 9.21 and 10.81 ms for the chirps at 40, 30 and 20 dB SPL, respectively. For identification purposes they are referred along the text as ABR–chirps.

Clicks: For the click stimulation, unit impulses with alternating polarity and a duration of 100 μsec were used.
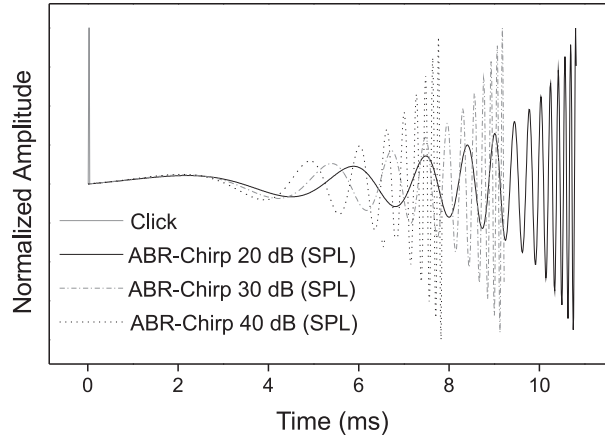
Figure 2.1: Waveforms of the ABR–chirps and click. The ABR–chirps were calculated with a frequency range of 0.1-10kHz, and different intensity levels: 40, 30, and 20 dB SPL. From right to left, chirp for 20 dB SPL(black continuous line), chirp for 30 dB SPL (gray dot-dashed line), chirp for 40 dB SPL (gray dashed line) and click of 100 μsec (gray continuous line).

All stimulation waveforms are shown in Fig. 2.1. For all stimulation conditions the repetition rate was 20 Hz. All the stimuli were calculated digitally and converted to a sound file with a sampling frequency of 44.1 kHz.

2.1.2   Study 2: Notched–Noise Embedded Frequency Specific Chirps

Chirps Series: Based on the chirp created and tested by Dau et al. (2000b); Fobel and Dau (2004) (where the latency–frequency function was developed on the basis of the linear cochlear model of de Boer and the cochlear frequency–position functions obtained by Greenwood in Greenwood (1990)), a broadband chirp was generated for the frequency range of 0.1–10 kHz (central frequency: 5250 Hz). The chirp was calculated following the same procedure as for the ABR–chirps, using Eq. (2.1.2), (2.1.3), and (2.1.4), but with the latency–frequency function:

$$\tau_{\text{BM}}(f) = k(f+a)^{-d} \tag{2.1.5}$$

with $k = 4.78$, $a = 165.4$ Hz, $d= 1.1$, und $t_o=\tau_{\text{BM}}$ (100 Hz), as reported by Elberling

et al. (2007).

Next, the series of chirps was developed using the same total operation range of 9.9 kHz (0.1–10 kHz). This range served to generate the 5 bands (2^n, n $\in \{1, 2, \ldots, 5\}$) for the frequency specific chirps. The bands were then centered on standard frequencies for audiograms, see theoretical (calculated) values in Tab. 2.1. In ascending order, the smaller bands correspond to the low central frequencies and the larger bands correspond to the higher central frequencies, respectively. The rational here is to combine an amplitude envelope that results in a flat frequency spectrum stimulus, like in Dau et al. (2000b), combined with notched–filtered masking noise. With the previously stated and ensuring that each stimulus starts and ends with zero, it is presumed that the effect of an abrupt onset or offset is then diminished. Therefore the chirps were adjusted to the latency–frequency function in order to have zero values at their beginning and at their end.

It was also desirable that the chirps would have as many cycles as possible. Thus, the duration criteria, besides the condition of 0 at the beginning and at the end, was taken according to have at least a minimum number of cycles. In Wegner and Dau (2002) the authors used a "3–half–waves" chirp, which was also took as criteria here for the minimum number of half cycles to have in the chirps. The final bands were slightly different from the first calculated ones (in general the frequencies changed less than 20%), and they remained under the tolerance limits according to the initial values, see Tab. 2.1.

Table 2.1: Calculated and final (') parameters of the frequency specific chirps. With a Range of 9.9 kHz.

Chirp number	Bandwidth (Hz)	Fc (Hz)	Interval (Hz)	Fc' (Hz)	Interval' (Hz)	Bandwidth' (Hz)	duration (ms)
1	Range/$2^5 \equiv 309$	250	[95, 405]	302	[108, 490]	382	6.1946
2	Range/$2^4 \equiv 619$	750	[441, 1059]	813	[495, 1135]	640	2.0185
3	Range/$2^3 \equiv 1238$	2000	[1381, 2619]	1915	[1230, 2600]	1370	0.87806
4	Range/$2^2 \equiv 2475$	4000	[2763, 5238]	6725	[2950, 10500]	7550	0.5091
5	Range/$2^1 \equiv 4950$	8000	[5525, 10475]	–	–	–	–
Broadband	Range/$2^0 \equiv 9900$	5050	[100, 10000]	5050	[100, 10000]	9900	10.12

A special consideration has been done for the two chirps that had the higher frequency bands. The ranges (of both chirps) were added, and one chirp instead of two was constructed. Therefore we had finally 4 frequency specific chirps. The reason to design this one chirp out of two was because the model did not allowed the criteria of "3–

half–waves" for the two last high-frequency chirps. Therefore a fourth chirp covered the ranges of both chirps. This limitation of the latency–frequency function and possible improvements will be discussed in later sections as well as in the Chapter 4.

The final waveforms, as well as the latency–frequency function can be seen in the Fig. 2.2. In the same figure and in Tab. 2.1, the numerical values of the final central frequencies, frequency bands, intervals and duration of the chirps are shown. For identification purpose, the chirps are called Ch1, Ch2, Ch3, and Ch4, according to their frequency range, where Ch1 is for the stimulus with the lowest frequency band and Ch4 is for the chirp with the highest frequency band. For the broadband chirp the abbreviation is B–bCh.

It is important to mention that the final chirps included the standard audiogram frequencies inside their frequency range.

Notched Masking Noise: For the notched masking noise files, white noise as recommended in Stapells (1994), was created using the software MATLAB (The MathWorks Inc., USA). The noise was band–passed filtered for the frequency range of 0.1–10 kHz, afterwards it was notched filtered using digital finite impulse response filters. A noise file was calculated for every chirp. The cut–off frequencies of these notch filter files fitted the limits of their respective chirp. The noise in all conditions was 20dB below the corresponding pe SPL intensity of the chirps (Stapells, 1994). After calibration, for details of the calibration procedure see Sec. 2.1.3, the noise and the stimuli were converted to a single sound file and then presented to the subject. Note that the noise was not added to the broadband chirp as in this case it was intended to stimulate the entire cochlea.

All the chirps had alternating polarity (one time the stimuli started with positive values the next time with negative values) and a repetition rate of 20 Hz. All the stimuli were calculated digitally and converted to a sound file with a sampling frequency of 44.1 kHz.

2.1.3   Stimuli Calibration

The setup and stimuli were calibrated according to European Committe for Standardization (2007); International Organization for Standarization (2007); Richter and Fedtke (2005). For this purpose, the peak equivalent (pe) SPL had to be calculated for
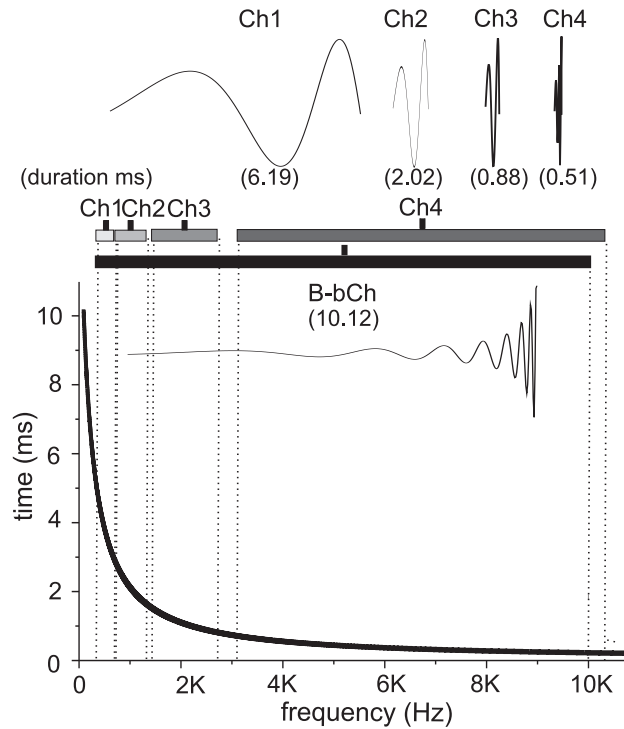
Figure 2.2: Frequency specific chirps. Thick black line: latency–frequency function, which served for the generation of the chirps. The resulting waveforms, frequency bands, and duration of the chirps are also shown. Here, Ch1 corresponds to the chirp with the smallest and lowest frequency band and Ch4 corresponds to the chirp with the highest and largest frequency band. B–bCh is a broadband chirp, which covers the entire frequency range.

each type of stimulus. The peak voltages were measured using a digital oscilloscope (TPS 2014, Tektronix, USA), and the equivalent reference sinusoidal waves (to calculate the pe SPL) were produced by a function signal generator (33220A, Agilent, USA). A sound level meter (type 2250, Brüel & Kjær, Denmark) measured the different pe SPL values via a prepolarized free field 1/2" microphone (type 4189, Brüel & Kjær, Denmark) connected to an artificial ear (type 4153, Brüel & Kjær, Denmark). The artificial ear was simultaneously coupled to the headphones (HDA–200, Sennheiser, Germany) while reproducing the reference sinusoidal waves.

2.2 Experimental Procedure, and Subjects

2.2.1 Measurement Setup and Preprocessing

The Fig. 2.3 shows the experimental setup used for the acquisition of the ABRs. A personal computer controlled the acquisition of the electroencephalographic activity, and the presentation and intensity level of the stimuli. The electroencephalographic activity was acquired by a high–end 24 bit biosignal amplifier (g.USBamp, g.tec, Austria) using a sampling frequency of 19.2 kHz, and a band–pass filter with low and high cut–off frequencies of 0.1 and 1.5 kHz, respectively. The biosignal amplifier was connected via USB port to the computer. The intensity level was controlled by means of a programmable attenuator buffer (g.PAH, g.tec, Austria) connected to the computer via serial port. Each sound file was generated together with its respective trigger signal. The audio channel that corresponded to the stimuli was connected to the attenuator and afterwards delivered to the subject via circumaural headphones (HDA–200, Sennheiser, Germany). The trigger channel was connected to a trigger conditioner box (g.Trigbox, g.tec, Austria) which adapted the voltage level of the trigger signal in order to be acquired by the biosignal amplifier. The acquisition–processing program and all further post–processing were achieved using software for technical computing (MATLAB–Simulink, MathWorks Inc., USA).

The following electrode placement was performed for all the measurements: ipsilateral to the stimulus at the right mastoid (A1), common reference at the vertex (Cz) and ground at the upper forehead (Fpz). The electrode labels are according to the standard 10–20 system. Impedances were maintained below 5kΩ in all the measurements.

2.2.2 Study 1: Chirps vs Clicks and Active vs Passive Electrodes

Electrodes: Two different types of sintered Ag/AgCl electrodes were used during the experiments: passive (Schwarzer GmbH, Germany) and active, impedance–converting–amplification electrodes (EASYCAP GmbH, Germany), e.g., see Hagemann et al. (1985) for a more detailed discussion on active electrodes. Electrodes were placed as described in Sec. 2.2.1.
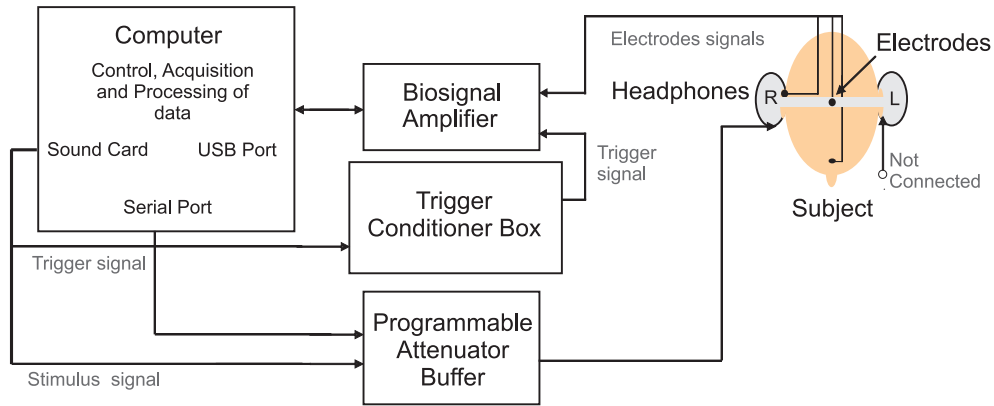
Figure 2.3: Setup for the acquisition of ABRs. The computer controls: (a) the acquisition of the electroencephalographic activity via USB port using a biosignal amplifier; (b) the intensity of the stimuli via serial port by using a programmable attenuator buffer; (c) stimuli and trigger signals presentation. The trigger signal is processed prior acquisition by a trigger conditioner box. The software developed for the specific purpose acquires, filters and stores the data.

Experiment: The time for one complete experiment was approx. 1.5 h including the time for the preparation of the subject and electrodes placement. Active electrodes were attached first. Subjects were instructed to lay on a bed in an acoustically insulated room trying to remain quiet, with the eyes closed, and sleep if possible. After the headphones were placed, the impedances were verified, and the lights were turned off.

Subsequently, ABRs were obtained using clicks for the intensity levels of 40, 30, 20 dB pe SPL, and the spontaneous activity for the same time segments (i.e., number of samples) that were used in the stimulated condition. In other words, in this way we obtained single sweeps of the spontaneous activity.

Later the ABR–chirps were presented for the same intensity levels and in the same order. Soon after, the electrodes were removed, and after skin preparation the passive electrodes were placed, and the same stimulation procedure was applied as for the active electrodes. In total 16 files were recorded. In each recording and condition 2000 sweeps free from amplitude artifacts (artifacts were removed by an amplitude threshold (15μV) detection; not more than 10% of artifacts were in the obtained single sweep sequences for all the subjects, electrodes, and stimulation conditions) were recorded. The measurement sequence was identical for each subject.

Subjects: Twenty volunteers (mean age 24.45 years with a standard deviation of 3.80 years; 13 female, 7 male) with no history of hearing problems and normal hearing thresholds (below 15 dB (HL)) as checked by an audiogram participated in the experiments. After a detailed explanation of the procedure, all subjects signed a consent form.

2.2.3 Study 2: Notched–Noise Embedded Frequency Specific Chirps

Experiments: The time for one complete experiment was approx. 2.0 h including the time for the preparation of the subject and electrodes placement. Passive Ag/AgCl electrodes (Schwarzer GmbH, Germany) were attached as described in Sec. 2.2.1. The subjects were instructed to lay on a bed in an acoustically insulated room trying to remain quiet, with the eyes closed, and sleep if possible. The headphones were placed and after verifying correct impedances, the lights were turned off. Subsequently, ABRs were obtained using the broadband chirp and next, using the notched–noise embedded frequency specific chirps for the intensity levels of 50, 40, and 30 dB pe SPL. In total 15 files were recorded. In each recording and condition 3000 sweeps free from amplitude artifacts (artifacts were removed by an amplitude threshold (15μV) detection) were recorded. The measurement sequence was identical for each subject.

Subjects: The data was collected from ten volunteers (mean age 25.1 years with a standard deviation of 2.96 years; 4 female, 6 male), with no history of hearing problems and normal hearing thresholds (below 15 dB (HL)) as checked by an audiogram carried out before the experiments. After a detailed explanation of the procedure, all subjects signed a consent form.

2.3 Inter-Sweep Phase Synchronization Measures

The application of mathematical transformations to signals is performed in order to get information that is not accessible in the original domain mostly time domain, of the signal. Many different approaches have been developed for the assessment of frequency analysis of transient biomedical signals, i.e., complex wavelet transform (CWT), window fourier transform (WFT), Gabor frames (GFs), among others.

For the present work, the focus is on two time–frequency decomposition techniques: CWT and GFs.

2.3.1   Wavelet Transform and Wavelet Phase Stability

Wavelet Transform: The wavelet transform has been introduced as a new mathematical tool for signal analysis (Goupillaud et al., 1984; Daubechies, 1992; Vetterli and Kovačević, 1995) and has already had a large impact on biosignal processing, see Akay (1997). As mentioned before, it provides a time–scale (the scale is linked to a frequency range) representation of transient signals and the main motivation for its application in biosignal processing is the fact that the most interesting features of such signals are simultaneously localized in time and scale, for instance, waveforms in electroencephalographic (EEG), e.g., evoked potentials.

Here a short introduction to the wavelet transform is provided, which is also necessary for further discussion. More details can be found in Daubechies (1992) and Vetterli and Kovačević (1995). Let us consider a function $\psi \in L^2(\mathbb{R})$ where $L^2(\mathbb{R})$ denotes the Hilbert space of all square integrable functions, i.e., all functions x that satisfy $\int_{\mathbb{R}} |x(t)|^2 \mathrm{d}t < \infty$. The function ψ is called a *wavelet* if it satisfies the following *admissibility condition*

$$0 < \int_{\mathbb{R}} |\Psi(\omega)|^2 |\omega|^{-1} \mathrm{d}\omega < \infty, \qquad (2.3.6)$$

where Ψ is the Fourier transform of ψ. This condition implies that $\Psi(0) = \int_{\mathbb{R}} \psi(t)\mathrm{d}t = 0$, i.e., the wavelet oscillates such that it has a zero mean. By the translations and dilations of the 'prototype' wavelet ψ, we obtain the doubly–indexed family functions

$$\psi_{a,b}(\cdot) = |a|^{-1/2}\psi((\cdot - b)/a), \qquad (2.3.7)$$

where $a, b \in \mathbb{R}$, $a \neq 0$. The wavelet transform $\mathcal{W}_\psi$ which maps a function $x \in L^2(\mathbb{R})$ into the time–scale domain is given by the inner L^2–product

$$(\mathcal{W}_\psi x)(a,b) = \langle x, \psi_{a,b} \rangle_{L^2} = \int_{\mathbb{R}} x(t)\psi_{a,b}^*(t)\mathrm{d}t, \qquad (2.3.8)$$

where the asterisk denotes complex conjugation. Unlike sine and cosine which comprise the basis functions of the Fourier transform, wavelets are characterized by a fast decay or compact support, i.e., they are essentially limited to a finite interval. Thus (2.3.8)

provides information about features which are local in time. The scale parameter a in (2.3.7) controls the dilation of the wavelet ψ and b its translation in time. For large values of a, the wavelet $\psi_{a,b}$ covers a large time interval and $(\mathcal{W}_\psi x)(a,b)$ yields a global view of f with a high sensitivity for low–frequency components, see Fig. 2.4 for the representation of WT in the time–frequency plane. For small values of a, the transform $(\mathcal{W}_\psi x)(a,b)$ provides information about short high–frequency components of x. In contrast to other time–frequency analysis techniques, e.g., the *windowed Fourier transform* (Daubechies, 1992), the wavelet transform analyzes with a variable window in the time–frequency domain by the described dilations of the wavelet. In this way, a better compromise between the time and frequency resolution can be achieved in comparison to the fixed window of the windowed Fourier transform (Daubechies, 1992; Vetterli and Kovačević, 1995).
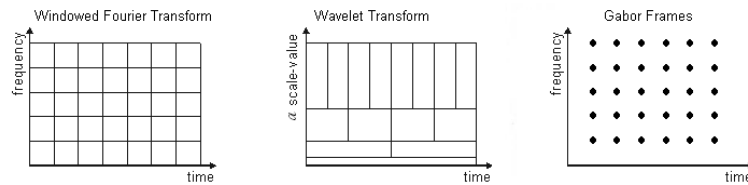
Figure 2.4: Different time–frequency domain representations. Left: Windowed fourier transform (WFT); Center: Wavelet transform (WT); and Right: Gabor frames (GFs). Note that for WFT the time–frequency resolution is fixed, whereas for WT it is variable and depends on the value of the scale a, a small value of a decreases time spread but increases frequency resolution, and viceversa. In the case of the GF, the information is sampled on a less dense grid.

Wavelet Phase Stability: For the determination of the phase synchronization stability, we need an adaptation of the derived phase locking measure between two signals to our problem, see Lachaux et al. (1999).

In this study, the 6th–derivative of the complex Gaussian function was used as wavelet, see Louis et al. (1997) for more details and an introduction to wavelets.

Note that the scale a can always be associated with a 'pseudo' frequency f_a in Hz by $f_a = T f_\psi / a$, where T is the sampling period (the sampling frequency f_s used was 19.2 kHz, as described in Sec. 2.2.1) and f_ψ is the center frequency of the wavelet ψ (Abry, 1997).

The wavelet phase stability (WPS) $\Gamma_{a,b}$ of an ABR sequence $\mathcal{X} = \{x_m \in L^2(\mathbb{R}) : m = 1, \ldots, M\}$ of M sweeps is defined by

$$\Gamma_{a,b}(\mathcal{X}) := \frac{1}{M} \left| \sum_{m=1}^{M} e^{i \arg\left((\mathcal{W}_\psi x_m)(a,b)\right)} \right|. \tag{2.3.9}$$

Note that the synchronization stability in (2.3.9) is a value in $(0, 1)$. It is a perfect synchronization stability for a particular a' and b' for $\Gamma_{a',b'} = 1$ (perfectly coherent phases) and a decreasing stability for smaller values due to phase jittering.

2.3.2   Gabor Frames and Gabor Frame Phase Stability

In this section are introduced the necessary mathematical formalisms and notation for the Gabor phase stability analysis of ABRs. For a general introduction to discrete time frames the reader is referred to Strohmer (1999).

Frames and Frame Operators: In the following, the interest is restricted to discrete time systems and signals such that all signals are represented by sequences. For the sake of a handy notation, the index of the individual sequence elements is denoted as argument in square brackets. Let ℓ^2 denote the Hilbert space of all square summable sequences, i.e., $\ell^2 = \ell^2(\mathbb{Z}) = \{\mathbf{x} : \mathbb{Z} \mapsto \mathbb{C} : \sum_{m \in \mathbb{Z}} |x[m]|^2 < \infty\}$. The interest is further restricted to time–invariant systems of the form

$$\varphi_{m,n}[\cdot] = \varphi_m[\cdot - \alpha n], \quad n \in \mathbb{Z}, \, m = 0, 1, \ldots, M-1, \, \alpha \in \mathbb{N}_{>0}. \tag{2.3.10}$$

where $\boldsymbol{\varphi}_m \in \ell^2$. A set $\{\boldsymbol{\varphi}_{m,n} : m, n \in \mathbb{Z}, \, \boldsymbol{\varphi}_{m,n} \in \ell^2\}$ is called a frame for ℓ^2 if

$$A||\mathbf{x}||_{\ell^2}^2 \leq \sum_{m,n \in \mathbb{Z}} |\langle \mathbf{x}, \boldsymbol{\varphi}_{m,n} \rangle_{\ell^2}|^2 \leq B||\mathbf{x}||_{\ell^2}^2, \quad \forall \mathbf{x} \in \ell^2. \tag{2.3.11}$$

For $A = B$ the frame is called a *tight frame* for ℓ^2 and we have the expansion $\mathbf{x} = A^{-1} \sum_{m,n \in \mathbb{Z}} \langle \mathbf{x}, \boldsymbol{\varphi}_{m,n} \rangle_{\ell^2} \boldsymbol{\varphi}_{m,n}$. If $||\boldsymbol{\varphi}_m||_{\ell^2}^2 = 1 \, \forall m \in \mathbb{Z}$ and $A = 1$ we obtain orthonormal expansions and for $A > 1$ the expansion becomes overcomplete and A reflects its redundancy. Two frames $\{\boldsymbol{\varphi}_{m,n} : m, n \in \mathbb{Z}\}$ and $\{\tilde{\boldsymbol{\varphi}}_{m,n} : m, n \in \mathbb{Z}\}$ for the Hilbert space ℓ^2 are called *dual frames* if $\mathbf{x} = \sum_{m,n \in \mathbb{Z}} \langle \mathbf{x}, \boldsymbol{\varphi}_{m,n} \rangle \tilde{\boldsymbol{\varphi}}_{m,n}, \, \forall \mathbf{x} \in \ell^2$.

The frame operator $\mathcal{F} : \ell^2 \mapsto \ell^2$ of the frame $\{\boldsymbol{\varphi}_{m,n} : m, n \in \mathbb{Z}\}$ is defined by

$$(\mathcal{F}\mathbf{x}) = \sum_{m,n\in\mathbb{Z}} \langle\mathbf{x}, \boldsymbol{\varphi}_{m,n}\rangle \boldsymbol{\varphi}_{m,n}.$$

Condition (2.3.11) ensures that $\mathcal{F}$ is bounded and invertible on ℓ^2. The dual frame $\{\tilde{\boldsymbol{\varphi}}_{m,n} : m,n \in \mathbb{Z}\}$ of the time–invariant system $\{\boldsymbol{\varphi}_{m,n} : m,n \in \mathbb{Z}\}$ is given by

$$\tilde{\varphi}_{m,n}[\cdot] = \left(\mathcal{F}^{-1}\varphi_m\right)[\cdot - \alpha n], \tag{2.3.12}$$

where $\mathcal{F}^{-1}$ is the inverse frame operator.

Gabor Frames: A Gabor system $(\boldsymbol{\varphi}, \alpha, M^{-1})$ for ℓ^2 is defined as

$$\varphi_{m,n}[\cdot] = e^{2\pi\imath m\cdot M^{-1}}\varphi[\cdot - \alpha n], \tag{2.3.13}$$

i.e, the system represents a family of sequences which are generated by one particular sequence due to modulation and translation. A Gabor system that is also a frame for ℓ^2 is called a *Gabor Frame* for ℓ^2. For $\alpha M^{-1} > 1$ the system is undersampled and cannot be a basis or a frame for ℓ^2. For $\alpha M^{-1} = 1$ it is the critically sampled case and, if the Gabor system represents a frame, it is also a basis. For $\alpha M^{-1} < 1$ it is the oversampled case and the Gabor system cannot be a basis but a frame. In this work, we deal with the latter case, see Fig. 2.4 for an example of its representation in the time–frequency plane.

An important property of Gabor frames is that the dual frame is also generated by a single sequence such that

$$\tilde{\varphi}_{m,n}[\cdot] = e^{2\pi\imath m\cdot M^{-1}}\tilde{\varphi}[\cdot - \alpha n], \tag{2.3.14}$$

with $\tilde{\boldsymbol{\varphi}}_{m,n} = \mathcal{F}^{-1}\boldsymbol{\varphi}_{m,n}$.

Note that the Gabor frame operator $\mathcal{F}$ is a combination of the analysis and synthesis operators that are introduced in the following, e.g., see Strohmer (1999). Let us introduce the index set $\mathcal{I} = \{0, 1, \ldots, M-1\}$. The Gabor frame analysis operator $\mathcal{G}_\varphi : \ell^2 \mapsto \ell^2(\mathcal{I} \times \mathbb{Z})$ is defined by

$$(\mathcal{G}_\varphi\mathbf{x})[m,n] = C[m,n] = \langle\mathbf{x}, \boldsymbol{\varphi}_{m,n}\rangle_{\ell^2}. \tag{2.3.15}$$

The Gabor synthesis operator $\mathcal{G}_{\tilde{\varphi}}^* : \ell^2(\mathcal{I} \times \mathbb{Z}) \mapsto \ell^2$ is defined by

$$x[\cdot] = \left(\mathcal{G}_{\tilde{\varphi}}^{*} C[m,n]\right)[\cdot] = \sum_{m,n\in\mathbb{Z}} C[m,n]\tilde{\varphi}_{m,n}[\cdot]. \tag{2.3.16}$$

The described Gabor decompositions can also efficiently be implemented by oversampled uniform band discrete Fourier transform filter banks as shown in Bölcskei et al. (1998).

Table 2.2: Analyzed intervals for the different stimulations according to the intensity. The analysis interval for each chirp starts after 3 ms of its respective duration, and ends after 7 ms.

Intensity dB (pe SPL)	Interval $[b_l, b_u]$ (ms)
Clicks 40	[5,11]
Clicks 30	[5,11]
Clicks 20	[5,11]
ABR–Chirp 40	[10.84,17.84]
ABR–Chirp 30	[12.21,19.21]
ABR–Chirp 20	[13.81,20.81]

Gabor Frame Phase Stability: Let $\mathbf{x}$ denote the analytic signal of an ABR single sweep, i.e., $\mathbf{x} = \mathbf{s} + \imath\mathcal{H}\mathbf{s}$ where $\mathbf{s}$ represents the original ABR single sweep waveform and $\mathcal{H}$ the Hilbert transform operator. Given the sequence $\mathcal{X}^{I} = \{\mathbf{x}_{k}^{I} \in \ell^{2} : k = 1, \ldots, K\}$ of analytic signals of K ABR single sweeps obtained at stimulation intensity I, the synchronization stability, represented by Gabor frame phase stability (GFPS) is defined by

$$\Gamma_{m,n}^{J}(\mathcal{X}^{I}) := \frac{1}{J}\left|\sum_{k=1}^{J} e^{\imath\arg\left((\mathcal{G}_{\varphi}\mathbf{x}_{k}^{I})[m,n]\right)}\right|, \quad J \leq K, \tag{2.3.17}$$

with $m \in \mathcal{I}$ and $n \in \mathcal{S} \subset \mathbb{Z}$. For a fixed modulation index m, the moving average representation (over the sweeps) of the GFPS in Eq. (2.3.17), is defined by the sequence

$$\Lambda_{m,n}^{I}[J] = \left(\Gamma_{m,n}^{1}(\mathcal{X}^{I}), \Gamma_{m,n}^{2}(\mathcal{X}^{I}), \ldots, \Gamma_{m,n}^{J}(\mathcal{X}^{I})\right). \tag{2.3.18}$$

In the further analysis, the interest is restricted to the time intervals where most of the energy of the ABRs was induced for the collected data segments, see Tab. 2.2. Let $\mathcal{U}^{I} \subset \mathcal{S}$ denote the associated sampling space, i.e., the set of samples that corresponds to these intervals. Then Eq. (2.3.18) averaged for this sampling space is given by

$$\overline{\Lambda}_{m}^{I}[J] = |\mathcal{U}^{I}|^{-1}\sum_{n\in\mathcal{U}^{I}} \Lambda_{m,n}^{I}[J]. \tag{2.3.19}$$

In other words, Eq. (2.3.19) represents the moving average (over the J sweeps) of the mean (for a fixed modulation index m) ABR GFPS (MAGPS).

2.4   A Hybrid Detection Scheme

In this section, the implementation of a hybrid detection scheme using the phase synchronization feature, which was introduced in the last sections, as well as a hybrid adapted filter bank – kernel based novelty detection scheme is discussed. For this, the very same data as in Sec. 2.1.1 (Study 1) was used, for the ABR–chirp stimulation at 30 dB pe SPL and active electrodes, which is a possible setup for screening applications. See Appendix A for a more detailed technical introduction to filter banks and kernel machines.

2.4.1   Adapted Filter Bank Based Feature Extraction

A hybrid wavelet–support vector classification has been introduced in Strauss and Steidl (2002) which employs lattice structure based wavelet and frame decompositions for feature extraction tasks in waveforms which are tailored for support vector classifiers with radial kernels. In particular, it provides a feature extraction which allows for an inclusion of a priori knowledge and leads to a maximal margin of the scheme, and is thus conform with the maximal margin theorem (Vapnik, 1995) of statistical learning theory.

The objective here is novelty detection (Tax and Duin, 1999) instead of binary classification. Nevertheless, the feature extraction stage is closely related to classification.

The original wavelet–support vector classifier as proposed in Strauss and Steidl (2002) relies on *multilevel concentrations* $\xi(\cdot) = || \cdot ||_{\ell^p}^p$ $(1 \leq p < \infty)$ of coefficient vectors of adapted wavelet or frame decompositions as feature vectors, i.e, scale features. These feature vectors incorporate the information about local instabilities in time as a priori information. For the classification of ABRs, we also include the morphological information of the waveforms as features as the discriminant information which separates the physiological and pathological sweeps is also reflected in the transient evolution of ABRs.

Since we are interested in a shift–invariant classification scheme, we may only evaluate the morphology of ABRs as a whole and not the exact latency of transient features. A possible way to realize this is by the use of entropy which is already employed to evaluate the subbands of wavelet and wavelet packet decompositions for the purpose of signal compression, see Coifman and Wickerhauser (1992) and Wickerhauser (1994). When using an appropriate entropy in connection with the tight frame decompositions, it is invariant to shifts of the sweeps. We define the entropy of a sequence $\mathbf{x} \in \ell^2$ by

$$E(\mathbf{x}) = -\sum_{n \in \mathbb{Z}} \frac{|x[n]|^2}{||\mathbf{x}||_{\ell^2}^2} \ln \frac{|x[n]|^2}{||\mathbf{x}||_{\ell^2}^2}. \qquad (2.4.20)$$

Note that $E(\cdot)$ is also the well known *Shannon entropy* (Cover and Thomas, 1991) but one where the probabilistic events are replaced by normalized energies of the samples, i.e., we do not deal with the probabilistic concept of the entropy here.

For a fixed ABR single sweep $\mathbf{x}$, we define the function

$$\begin{aligned} \boldsymbol{\zeta}^{\mathbf{x}}(\boldsymbol{\vartheta}) &= (\zeta_1^{\mathbf{x}}(\boldsymbol{\vartheta}), \ldots, \zeta_{2J}^{\mathbf{x}}(\boldsymbol{\vartheta})) \\ &= \left(||\mathbf{d}_1^{\boldsymbol{\vartheta}}||_{\ell^1}, \ldots, ||\mathbf{d}_J^{\boldsymbol{\vartheta}}||_{\ell^1}, E(\mathbf{d}_1^{\boldsymbol{\vartheta}}), \ldots, E(\mathbf{d}_J^{\boldsymbol{\vartheta}}) \right), \end{aligned}$$

and set $\boldsymbol{\zeta}^i(\boldsymbol{\vartheta}) := \boldsymbol{\zeta}^{\mathbf{x}_i}(\boldsymbol{\vartheta})$ $(i = 1, \ldots, M)$. Here $\mathbf{d}_j^{\boldsymbol{\vartheta}}$ denotes the coefficients of a shift–invariant lattice structure based octave–band tight frame decomposition, parameterized by the angle vector $\boldsymbol{\vartheta}$, see Appendix A. The number J is the decomposition depth. The first J elements of this feature vector carry multilevel concentration of the subbands in ℓ^1, i.e., a scale information. The second J elements carry the morphological information reflected in the entropy as defined in (2.4.20). Note that $\boldsymbol{\zeta}_i(\boldsymbol{\vartheta})$ is totally invariant against shifts of the individual sweeps. We used decomposition level 3 to 5 in this study as these levels carried the substantial signal information.

2.4.2   Kernel Based Novelty Detection

Suppose we are given a set of M samples and a description is required. We try to find a sphere with a minimum volume, containing all data in the hard case (no outliers in learning set) and most of the data in the soft case (the learning set may contain outliers). Instead of constructing this sphere in the original space, we construct it in a high dimensional feature space which is induced by a kernel of a reproducing kernel

Hilbert space (Wahba, 1999). All patters which lay outside the sphere are detected as novel instances which do not correspond to the learned class (Tax and Duin, 1999; Ben-Hur et al., 2001). The minimal sphere can be obtained by the following optimization problem:

$$\min_{\mathbf{a}\in\mathcal{F}_K, R\in\mathbb{R}, \mathbf{u}\in\mathbb{R}^M} R^2 + \lambda \sum_{i=1}^M u_j \tag{2.4.21}$$

subject to

$$||\mathbf{\Phi}(\boldsymbol{\zeta}_i(\boldsymbol{\vartheta})) - \mathbf{a}||^2 \quad \leq \quad R^2 + u_i \quad (i = 1, \ldots, M), \tag{2.4.22}$$
$$u_i \quad \geq \quad 0 \quad (i = 1, \ldots, M).$$

where the $\Phi : \mathcal{X} \subset \mathbb{R}^J \longrightarrow \mathcal{F} \subset \ell^2$ denotes the feature map from the pattern space to kernel feature space, $\mathbf{a}$ is the center of sphere (Tax and Duin, 1999), see Appendix A for an introduction to feature spaces induced by reproducing kernels.

For the embedding of the feature extraction in the minimal sphere approach above, the objective is now to find optimal lattice angles $\hat{\boldsymbol{\vartheta}}$ such that a learning set of M sweeps $\mathcal{A}(\boldsymbol{\vartheta}) = \left\{ \boldsymbol{\zeta}^i(\boldsymbol{\vartheta})) \in \mathcal{X} : i = 1, \ldots, M \right\}$ is as compact as possible in the feature space, i.e.,

$$\hat{\boldsymbol{\vartheta}} = \arg\min_{\boldsymbol{\vartheta}\in\mathcal{P}^2} \left\{ \sum_{i=1}^M ||\mathbf{\Phi}(\boldsymbol{\zeta}^i(\boldsymbol{\vartheta})) - \Xi||^2_{\mathcal{F}_k} \right\},$$

where $\mathcal{P}^2$ denotes the lattice parameter space for filters of order 5 (see Appendix A) and Ξ the feature center. For radial kernels of the SVM, problems of this type can be transformed from the feature to the original space and solved by genetic algorithms or a hypercube evaluation, see Strauss and Steidl (2002).

2.4.3   The Assembled Scheme

In order to combine the extraction of the phase synchronization stability of ABR sequences with the described kernel based novelty detection, we implemented the scheme in Fig. 2.5. Here the final decision is based on the result of the kernel machine for the filter banks as well as for the GFPS. For the GFPS, we used $\overline{\Lambda}^0_2[J]$ ($J \in \{21, 22, \ldots, 199, 200\}$ as a leaning set of 180 feature vectors. Note that we discarded here the first 20 sweeps due to large oscillations as described in Sec. 3.3. We
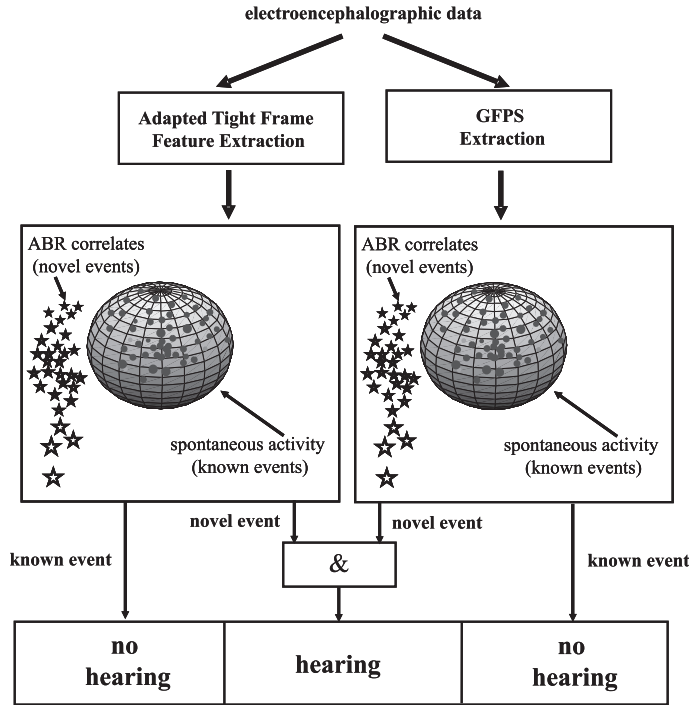
Figure 2.5: The assembled hybrid detection scheme.

selected the time interval for averaging the GFPS tighter (as compared to Tab. 2.2) such that this interval is represented by 20 samples, centered in the middle of the intervals in Tab. 2.2. We also subtracted a smooth fit of $\overline{\Lambda}_2^0[J]$ using an independent test set from all the feature vectors in the learning and testing sets for $I = 0$ and $I > 0$ in order to set these vectors close to a zero baseline.

Now a "real" novelty is detected if both kernel based novelty detection machines detect a novel instance. Note that this "AND" combination optimizes the system with respect to the sensitivity in view of its intended application in hearing screening. To end this, an abstract synchronization on brainstem level as large–scale neural correlate of a physiological hearing at intensity I is detected if both machines detect a novelty. Otherwise, no hearing correlate is detected.

For the all the experiments in Sec. 3.3, we used $J = 200$ sweeps as learning set and 200 sweeps for testing the spontaneous activity and stimulations at 30 dB SPL, respectively. It goes without saying that we used a different set of sweeps for the learning and testing phase in the case of the spontaneous activity.

Chapter 3

Results

In this Chapter the results obtained for the different tested paradigms are shown, ranging from the time domain waveforms to the post-processing results using different time–frequency analysis, as well as results of the novelty detection. The sections are organized according to the stimulation paradigm used to evoked the ABRs, as mentioned in Sec. 1.6.

For the first study, the following is reported: the time domain signals of the collected ABRs data evoked by clicks and ABR–chirps, their time–frequency analysis and their phase adjustment by using Gabor frames and GFPS.

For the second study, results of the development, testing, and evaluation of a series of notched–noise embedded frequency specific chirps to evoke ABRs in healthy subjects are reported. The ABRs collected here were analyzed using time–scale phase synchronization stability measures by means of wavelet transform and WPS.

Finally, the results of the novelty detection algorithm for the fast detection of single sweeps of ABRs are also shown.

3.1   Study 1: Chirps vs Clicks, and Active vs Passive Electrodes

3.1.1   Stimuli

The waveforms of the resultant ABR–chirps are shown in Fig. 2.1. Note the different durations of the ABR–chirps which are related to the intensity factors (the larger the intensity the shorter the duration and viceversa). In the same figure it can also be seen the amplitude envelope, which accomplish a flat spectrum by weighting the frequencies by their duration (the low frequencies last longer, and therefore their amplitudes were smaller as compared to high frequencies amplitudes, which had a shorter duration in time, and therefore their larger amplitudes compensated their contribution).

3.1.2   Auditory Brainstem Responses and Electrodes

Measurement examples of the ABRs collected from one subject (number 2) are shown in Fig. 3.1 as single sweep matrix representation, i.e., the amplitude of the sweeps is encoded in a gray–scale map, and as thick white lines the averaged time domain waveforms for different stimuli, intensities and different set of electrodes (active and passive). In the case of the chirps, their increased latencies due to their long durations are clearly noticeable as well as the stronger traces of wave V in the single sweep matrix representations. At first sight no influence from the different type of electrodes can be extracted from the potentials shown in the same figure. In all the subjects, identifiable waves V were found. For space reasons, only the ABR waveforms from one subject are reported, and the complete database with all the collected information is available if required.

Nevertheless, to summarize the relevant information related to the ABRs collected during the entire study, the wave V latencies for all the subjects and all the conditions are shown in Fig. 3.2. The left column shows the latencies considering the onset of the ABR–chirp stimulations, whereas the right column shows the latencies considering only the offset of the stimuli. Note that for the click stimulations the onset and the offset are considered as the same value (0 ms). The average overall the subjects, and standard deviations for every condition are also shown at the most left side of each
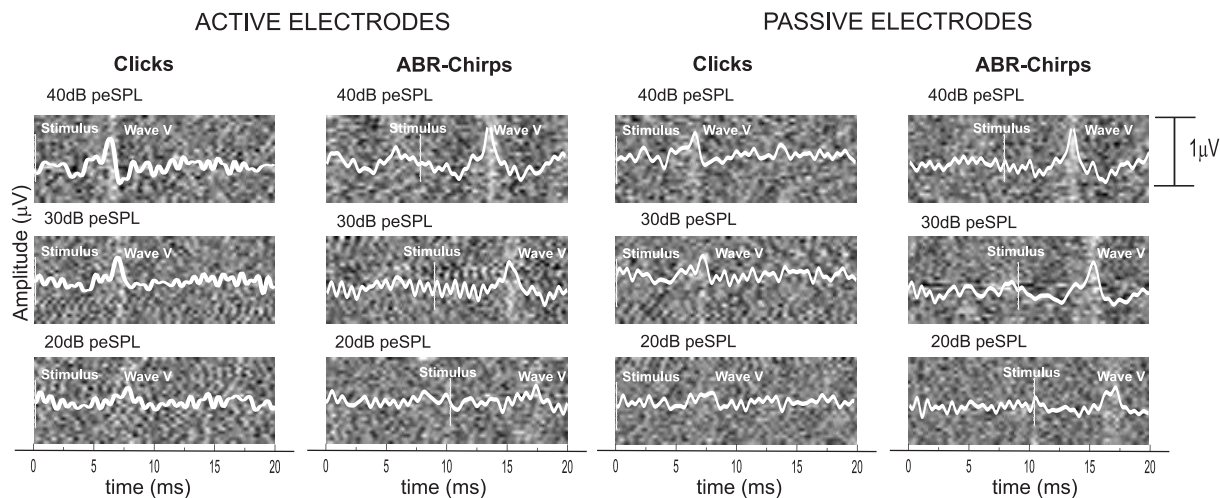
Figure 3.1: (Study 1) ABRs obtained from one subject (No. 2) for the different stimuli (clicks and ABR–chirps), intensity levels, and electrodes (passive and active). Each thick white line represents the average of a dataset of 2000 responses and it is plotted over the sweeps in matrix representation. Each line in the sweeps matrix representation is the average of 75 sweeps and the amplitude is coded in gray colors ranging from black (small amplitudes) to white (large amplitudes)). The end of the stimuli as well as the waves V are also identified. The trace of wave V in the matrix representation is easier to identify for the chirp stimulations.

plot (which would correspond to patient number 0). In the left column it can be seen that the latencies for the responses evoked by ABR–chirps at different intensities have a larger separation between themselves as for the latencies at different intensities using clicks. This is related to the duration of the applied stimulus.

It is worth to emphasize that in the following the interest is in the abstract time–frequency phase locking features of the ABR sweeps and not in their time domain morphology using waveform detection techniques.

3.1.3 Gabor Frame Phase Stability

For the experiments in this section, the Gaussian function was used to generate the family of functions in Eq. (2.3.13) and Eq. (2.3.14) with $M = 60$ modulations and $\alpha = 1$. Note that these values result in an overcomplete Gabor frame decomposition with $m = 0, 1, \ldots, M - 1$ (m is the modulation index) frequency channels spanning the
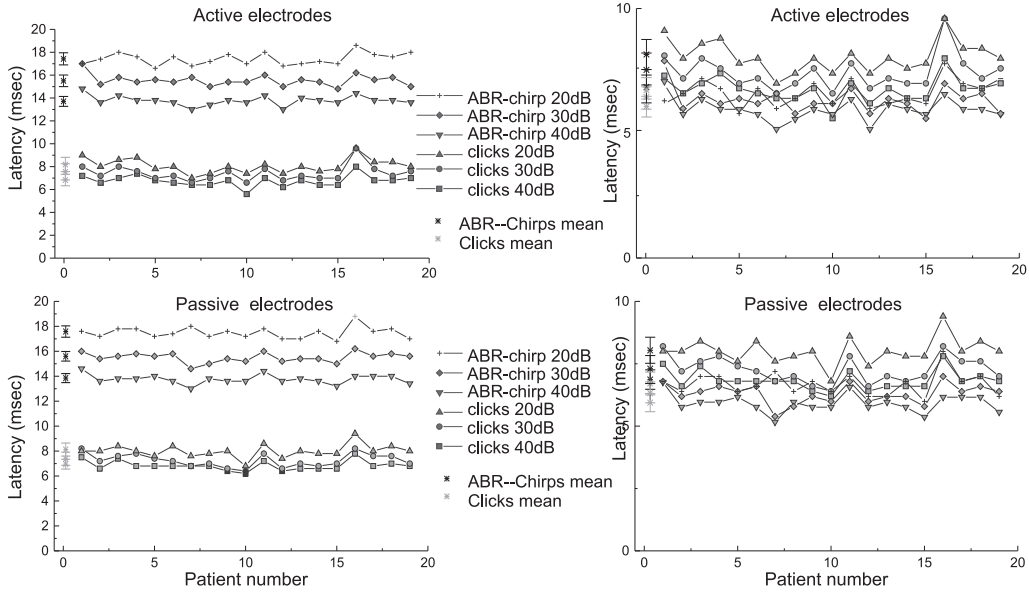
Figure 3.2: (Study 1) ABR wave V–latencies obtained from all the subjects, for the different electrodes conditions, stimulations (clicks and ABR–chirps) and intensity levels. Upper row: using for active electrodes. Bottom row: using passive electrodes. The left column shows the latencies considering the onset of the ABR–chirp stimulations, whereas the right column has the latencies considering only the offset of the stimuli. Note: for the click stimulations the onset and the offset are considered as the same value (0 ms). The means and standard deviations for every condition are shown at the left side of each plot (would correspond to patient number 0).

frequency interval $[mf_c, (m+1)f_c]$ with $f_c = f_s/(2M)$ (f_s is the sampling frequency $= 19.2$ kHz, as described in Sec. 2.2.1).

Results for Different Modulations: In the following the interest is restricted to the quantity $\overline{\Lambda}_m^I[J]$ in Eq. (2.3.19) for the spontaneous activity and 20 dB pe SPL stimulations by clicks and ABR–chirps for $m = 1, 2, 3, 4$, i.e., the modulations or bands in which most of the energy of the ABRs was induced in all the subjects. In Fig. 3.3 are shown the p–values for an (one–way) ANOVA (Shoukri and Pause, 1999) for comparing the means of $\overline{\Lambda}_m^I[J]$ for the spontaneous activity vs. 20 dB pe SPL stimulation over all the subjects, for each sample in time, and for an increasing sweep number ($J = 1000$). Figure 3.3 (top) shows the result for the click stimulation and Fig. 3.3 (bottom) for the ABR–chirp stimulation. With the exception of the high frequency channel $m = 4$, the chirp stimulation reaches significant p–values ($p < 0.05$) much earlier in time, i.e.,

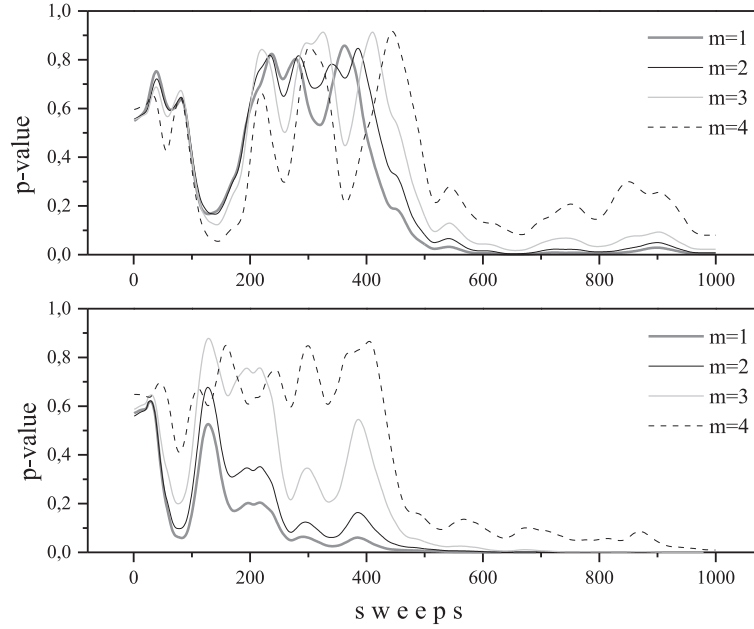for a much smaller number of sweeps, than the click stimulation, especially for $m = 1$.

Figure 3.3: (Study 1) Comparison of the means of $\overline{\Lambda}_m^I[1000]$ ($m = 1, 2, 3, 4$) for the spontaneous activity and for $I = 20$ dB SPL stimulations. Top: click stimulation; Bottom: ABR–chirp stimulation.

Performance Comparison Clicks vs. Chirps: In Fig. 3.4 it is shown the performance comparison between click and ABR–chirp stimulations for $m = 1$, different stimulation intensities, and passive electrodes. In particular, it is shown the mean of $\overline{\Lambda}_1^I[1000]$ over all the subjects in Fig. 3.4 (a) for clicks and in Fig. 3.4 (b) for the ABR–chirps. In Fig. 3.4 (bottom) the p–values for the (one–way) ANOVA significance test are shown for the spontaneous activity vs. stimulation, in Fig. 3.4 (c) for clicks and in Fig. 3.4 (d) for ABR–chirps. It is noticeable that the chirp stimulation converges for a much smaller number of sweeps (j) to significant ($p < 0.05$) values than the click stimulations. The very same analysis is presented in Fig. 3.5 for active electrodes with rather similar results.

Phase Stability in the Complex Plane: In Fig. 3.6 (a) it is shown the quantity $(\mathcal{G}_\varphi \mathbf{x}_k^I)[m, n]$ for $m = 1$ and a fixed sample n taken from the interval of wave V in line. More precisely, in this figure a complex number (with absolute value one) associated with a sweep $k + 1$ is "attached" (linearly translated with conserved absolute value and phase) to the complex number associated with sweep k (each straight line represents
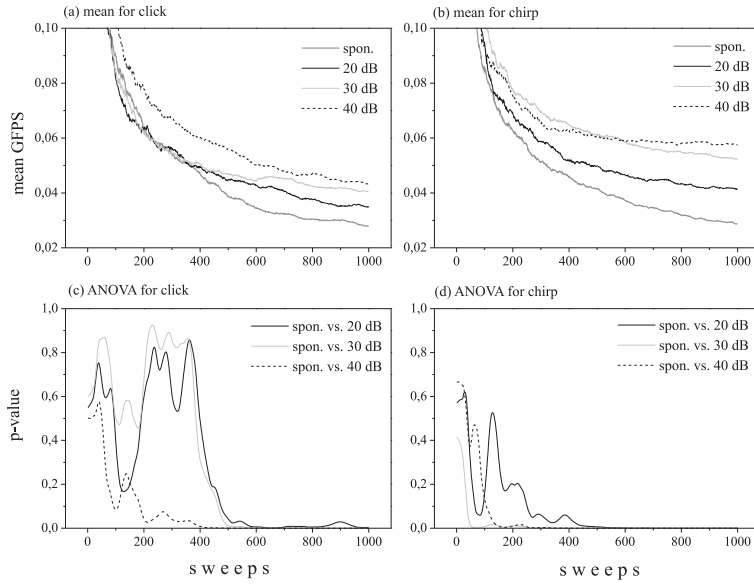
Figure 3.4: (Study 1) Results for passive electrodes and $m = 1$: (a): mean of $\overline{\Lambda}_1^I[1000]$ for the spontaneous activity and increasing click intensities; (b) mean of $\overline{\Lambda}_1^I[1000]$ for the spontaneous activity and increasing ABR–chirp intensities; (c) ANOVA for (a) and (d) ANOVA for (b).

one sweep in Fig. 3.6 (a)). The origin of the complex plane is marked by the circle. The very same number of 2000 sweeps is shown for the spontaneous activity and for the 30 dB pe SPL ABR–chirp stimulation. It is noticeable that the phase for the spontaneous activity is moving randomly around in the complex plane whereas the phase for the ABR–chirp stimulation is locked and exhibits stable angles, resulting in a large vector or smoother line, respectively, in the complex plane. It is easy to see that the application of the GFPS would yield a larger value in the latter case.

Phase Stability in the Time Domain: In order to show the influence of the phase stability in ABRs, the Gabor analysis and Gabor synthesis operator in Eq. (2.3.15) and Eq. (2.3.16) were used, respectively. At first, the analytic signals of a sequence of 2000 sweeps were decomposed by $\mathcal{G}_\varphi$. Then it was introduced an artificial phase stabilization by adjusting all the instantaneous phases (i.e., of each sweep) to the averaged instantaneous phase of 2000 sweeps. Let us describe this phase adjustment now more formally: it is denote the averaged instantaneous phase for sample n of the 2000 analytic signals by ξ_n. The phase for sample n of the analytic signal of each sweep is now adjusted by mapping it to the range $[\xi_n, \xi_n + \delta]$ where δ represents random noise
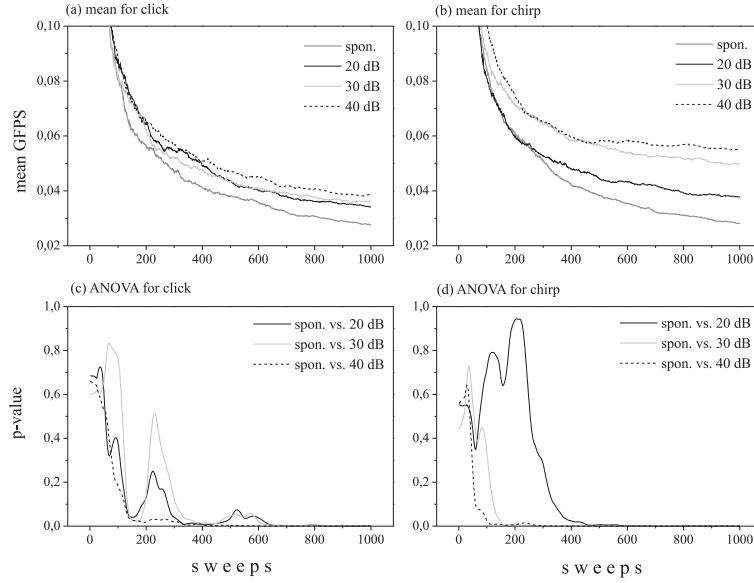
Figure 3.5: (Study 1) Results for active electrodes and $m = 1$: (a): mean of $\overline{\Lambda}_1^I[1000]$ for the spontaneous activity and increasing click intensities; (b) mean of $\overline{\Lambda}_1^I[1000]$ for the spontaneous activity and increasing ABR–chirp intensities; (c) ANOVA for (a) and (d) ANOVA for (b).

drawn from an uniform distribution on the interval $[0, 0.4]$ for $m = 2, 3$ and a fixed range in time (see the marked interval in Fig. 3.6(b, top)). The sequences modified in this sense are then mapped back to the original signal space by $\mathcal{G}_{\tilde{\varphi}}^*$. The original averaged ABR waveform $\mathbf{s}$, i.e., the real part of $\mathbf{x}$, evoked by ABR–chirps at 30 dB pe SPL as well as its phase adjusted version are shown in Fig. 3.6 (b, top). The time range of the phase adjustment is also marked in this figure. It is clearly noticeable that the phase adjustment results in a much larger and more clear waveform morphology. The effect of the phase adjustment is also clearly noticeable in the time domain single sweep matrix representation in Fig. 3.6 (b, bottom).
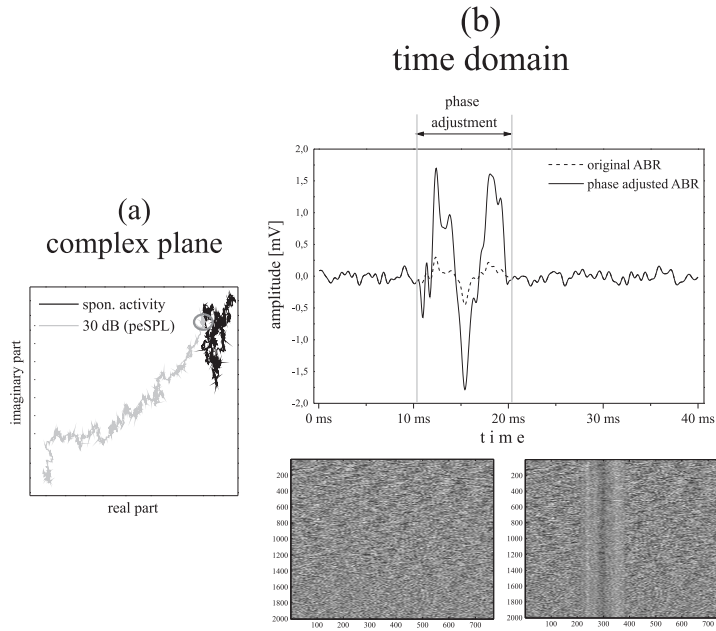
Figure 3.6: (Study 1) In the complex plane and time domain. (a): The quantity $(\mathcal{G}_\varphi \mathbf{x}_k^I)[m, n]$ for $m = 1$ and a fixed sample n taken from the interval of wave V. Each complex number (with absolute value one) is associated with a sweep $k + 1$, and is "attached" to the complex number associated with sweep k. The origin of the complex plane is marked by the circle. (b: top): The phase of the averaged original ABR waveform (dashed line) for 2000 sweeps is stabilized in the Gabor frame transform domain for the marked range. The synthesized (reconstructed) waveform is shown as black continuous line. (b: bottom–left): the single sweep matrix in the time domain for the original sweeps; (b: bottom–right): the single sweep matrix for the reconstructed phase adjusted sweeps.

3.2 Study 2: Notched–Noise Embedded Frequency Specific Chirps

3.2.1 Stimuli

The resultant series of chirps to evoked frequency specific ABRs are shown in Fig. 2.2. The different parameters, bands, durations are also shown in the Tab. 2.1. The final waveforms had at least "3–half–waves", and cover in a large proportion the total operation range. The latency–frequency function used to calculate the chirps is also

shown in the same figure. Note the longer duration for the low frequency–band chirps as compared to the higher frequency–band chirps.

3.2.2   Auditory Brainstem Responses

Examples of the measurements in one subject for the different conditions are shown in Fig. 3.7 as single sweep matrix representation, (as mentioned before the amplitude of the sweeps is encoded in a gray–scale, where white bright colors represent large values and dark colors represent small values), and as thick white lines, the averages for the time domain waveforms. Two lines are plotted for each condition. Each line represents the average of 1500 responses to show reproducibility as waveform. In the same figure the offset of the stimulus is subtracted, so the responses are aligned to the offset of their respective stimulus. The columns correspond to the responses for a specific intensity level (from left to right, 30, 40 and 50 dB pe SPL), and the rows 1, 2, 3, 4 and 5 correspond to the responses of Ch4, Ch3, Ch2, Ch1, and, B–bCh respectively. The 6th row is the addition of the responses from Ch1 to Ch4. And the last 7th row is the same addition but with prior alignment of the waves V.

Fig. 3.8 shows the latency–frequency function (black solid line) as well as the resulting values of the latency of the wave V, obtained from the grand average (overall the subjects), for the different chirps at the different intensity levels. Note that these averaged latency values are plotted in the center frequency of the corresponding chirp that was applied. Lines to connect the different averages are also plotted to make the recognition easier for the different intensities. The error bars represent the standard deviation. From top to bottom, light gray continuous line, dark gray continuous line and the gray dot–dashed linerepresent the intensities of 30, 40 and 50 dB pe SPL, respectively.

3.2.3   Wavelet Phase Stability

The Fig. 3.9 shows the grand average (overall the subjects) of the WPS for the different stimulation conditions, with M=3000 (sweeps), in (2.3.9). The columns correspond to the phase synchronization for a specific intensity level (from left to right, 30, 40 and 50 dB pe SPL), and the rows 1, 2, 3, 4 and 5 correspond to the chirps Ch4, Ch3, Ch2, Ch1, and, B–bCh, respectively. Dark gray to black and light gray to white colors
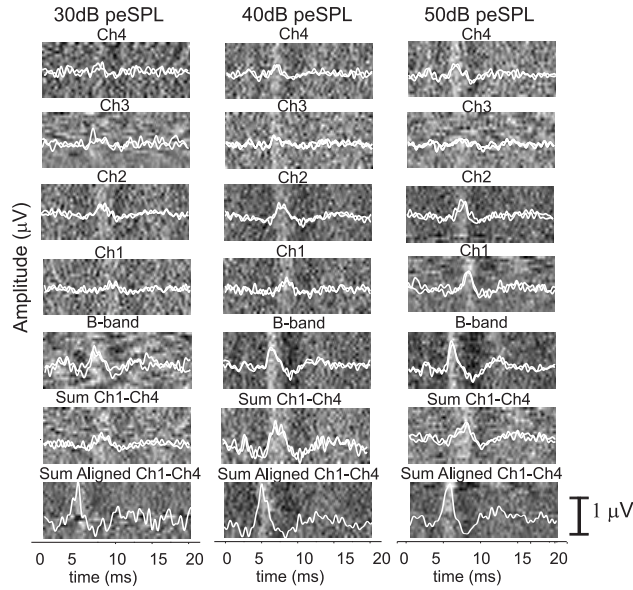
Figure 3.7: (Study 2) ABRs measurements collected from one subject for the different stimulation conditions –using the noise embedded frequency specific chirps. The columns correspond to the responses for a specific intensity level (from left to right, 30, 40 and 50 dB pe SPL), and the rows 1, 2, 3, 4 and 5 correspond to the responses evoked by the Ch4, Ch3, Ch2, Ch1, and B–bCh respectively. The row number 6 corresponds to the summation of the averaged responses of the ch1, ch2, ch3 and ch4, and the 7th row corresponds also to the same summation but after alignment of the waves V. Each average is represented by two white lines to show reproducibility, and they are placed above its respective single sweep matrix representation, i.e., the amplitude of the sweeps is encoded in a gray–scale map.

represent small and large values of WPS, respectively. For the calculations the value of the scale a ranged from 20 to 60 with increments of 5. In the same figure, Fig. 3.9, the latency shift of the wave V due to frequency specificity is easily noticeable in the synchronization stability, especially for middle to larger scales.
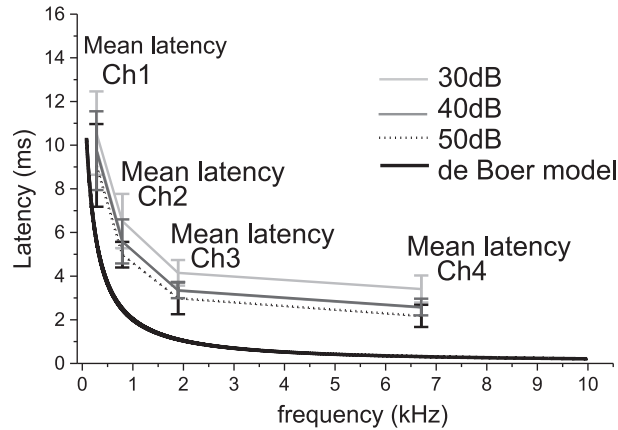
Figure 3.8: (Study 2) Wave–V Latency curves. Average latency values obtained from all the subjects and for all stimulation conditions –using the noise embedded frequency specific chirps. Light gray continuous line: for the intensity level of 30 dB pe SPL, dark gray continuous line: for the intensity level of 40 dB pe SPL, gray dot–dashed line: for the intensity level of 50 dB pe SPL, thick black line model of de Boer. For these curves, 5 ms were subtracted from the preliminary average value. Those 5 ms represents the neural component, which is not considered on the latency–frequency function, represented as a black thick line in the figure. The error bars indicate standard deviation.

3.3 Hybrid Detection Scheme

3.3.1 Filter Extraction Experiments

In Fig. 3.10 it is shown the discrete–time wavelets associated with level $j = 3, 4, 5$ of our parameterized decomposition scheme. In particular, these wavelets minimize the representation of the training data in feature space induced by a reproducing Gaussian kernel, see Eq. (2.4.22).

3.3.2 Kernel Based Novelty Detection

Two concentration features of our feature vector $\zeta^{\mathbf{x}}(\boldsymbol{\vartheta})$ are shown in Fig. 3.11 for the training sweep sequence of the spontaneous activity, an additional set of spontaneous activity sweeps (which was not included in the training date set), and for a stimulation above the hearing threshold (10 feature vectors are averaged to produce one
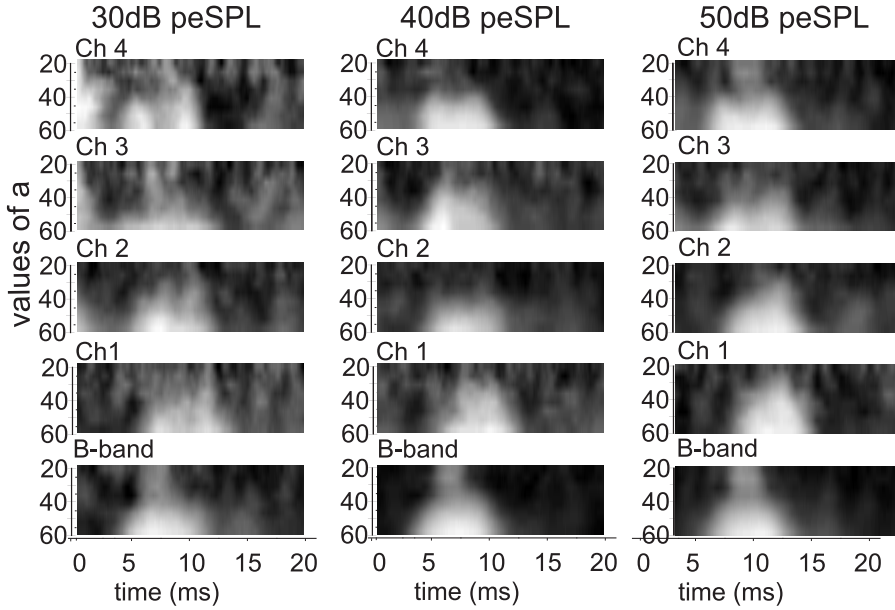
Figure 3.9: (Study 2) The grand average overall the subjects of $\Gamma_{a,b}(\mathcal{X})$ (the scale a ranges from 20 to 60 with increments of 5), for the different stimulation conditions, using the noise embedded frequency specific chirps. The left, center and right columns correspond to the intensity levels of 30, 40 and 50 pe SPL, respectively. The rows from top to bottom, correspond to the chirps Ch4, Ch3, Ch2, Ch1 and B–bCh, respectively. Dark gray to black colors and light gray to white colors represent small and large values of WPS, respectively.

representative feature vector for the kernel machine). It can be seen how the training data defines a nonlinear decision line in the pattern space which contains most of the spontaneous activity data (also those feature vector which were not included in the training set) and clearly separates the spontaneous activity from stimulations above the hearing threshold.

Using the scheme described in Sec. 2.4 and just $J = 200$ sweeps, ABRs can correctly be detected (i.e., a discrimination of sweeps with spontaneous activity which were not included in the training set and chirp–evoked ABRs) in 19 out of 20 patients at the challenging stimulation level of 30 dB pe SPL for the chirp stimulation.
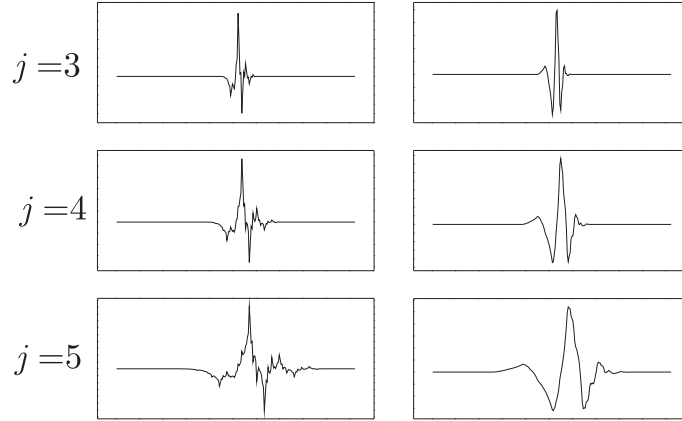
Figure 3.10: Discrete–time wavelets from the lattice angle space $\mathcal{P}$ which provide a minimal sphere in the kernel feature space for two different subjects. The wavelets are shown for decomposition level $j = 3, 4, 5$. The right column corresponds to the angles $\boldsymbol{\vartheta} = (1.89, 0.63)$ and the left column to $\boldsymbol{\vartheta} = (2.09, 2.09)$.
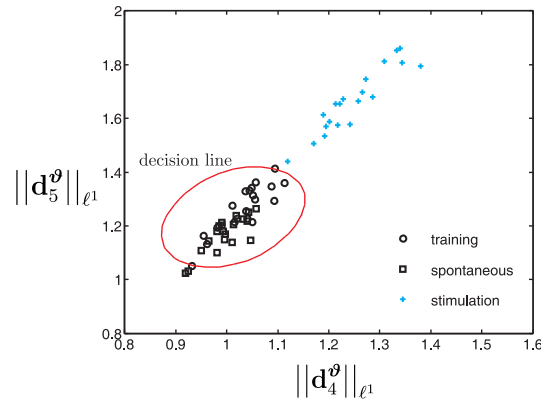
Figure 3.11: Two concentration features ($||\mathbf{d}_4^{\boldsymbol{\vartheta}}||_{\ell^1}$ and $||\mathbf{d}_5^{\boldsymbol{\vartheta}}||_{\ell^1}$) and the decision line as example for one subject. The circles denote training set of the novelty detection machine, the squares denote a set of spontaneous activity feature vectors which is different from the training set. The feature vectors corresponding to a stimulation above the hearing threshold are denoted by the gray + signs.

Chapter 4

Discussion

This chapter presents a detailed discussion of the results reported in the previous Chapter, using different stimulation conditions, post-processing methods, i.e., time–frequency analysis, and the novelty detection scheme.

The Chapter is organized as follows: first there is a section regarding the setup and its calibration; next, separated parts for study 1 and study 2 are discussed; followed by the section of the application and results of the novelty detection scheme; and finally there is a section of the possible future work that can be done, not only to improve the performance of the algorithms, but also related to the stimulation paradigms developed here.

4.1   Measurement Setup

The setup developed in order to acquire ABRs showed a good performance in general. The potentials were collected with a small number of artifacts in all the cases, and no interferences or problems were reported. The software that acquired and preprocessed the EEG data was also able to save the raw data. Therefore the chance to apply different digital filters, segmentation, and post-processing algorithms as part of future work is still possible.

In the cases where the impedance of the electrodes were not smaller than 5kΩ, the skin preparation was repeated. This happened for the passive electrodes in a small percentage of the subjects (approximately 20% of the subjects). In the case of the

active electrodes, the impedance values were always smaller, but a time gap (around 2–3 minutes) was always required at the beginning of each first measurement (first from the entire set) in order to collect sweeps without artifacts. The rest of the acquisition session went without problems. No explanation of this issue was reported in literature or by the manufacturers (Easycap GmbH, Germany).

The calibration of the setup was performed according to European Committe for Standardization (2007); International Organization for Standarization (2007); Richter and Fedtke (2005), and it was achieved by measuring the maximum pe SPL of the sound card used in the laptop that delivered the stimuli and performed the data acquisition. The procedure was the same as the one described for the stimuli in Sec. 2.1.3. The final intensity for the different stimuli during the measurements was controlled by the programmable attenuator buffer, as explained in Sec.2.2.1, where the possibility of attenuations in steps of 1 dB was possible. Taking this calibration procedure into account, we can make sure the reproducibility in further measurements.

pe SPL vs SL: In other studies reported in literature, the chirp stimuli were presented in dB sensation level (SL), which required the hearing threshold detection for each subject and for each type of stimulus. In order to avoid a subjective threshold adjustment every time when we had a different subject-stimulus combination, we obtain the pe SPL of every stimulus as specified in European Committe for Standardization (2007); International Organization for Standarization (2007); Richter and Fedtke (2005), for signals of short duration such as clicks and chirps.

4.2   Study 1: Chirps vs Clicks, and Active vs Passive Electrodes

4.2.1   Auditory Brainstem Responses, Stimuli, and Electrodes

Auditory Brainstem Responses, and Stimuli: The Fig. 3.1 shows ABR measurements collected from one subject. It can be seen that the potentials exhibit an identifiable wave V in all cases, and in specific for ABR–chirp stimulations, the waves V were even larger as compared with their respective waveforms at the same intensity

but evoked by clicks. These larger waves can be related to the duration, the spectral content, and temporal organization of the stimulus used to evoked the potentials.

On one hand, regarding the duration of the stimuli, the chirps last longer than the clicks and therefore more energy is implied in the generation of the response. On the other hand, by their design, both stimuli have a broad range of frequencies and a wide spectral content, as explained in Sec. 1.3. In contrast, the rising frequency of the chirp stimulation, see Fig. 1.3, takes the tonotopic organization of the cochlear into account. Thus, theoretically low frequencies would reach their sensation locus at the same time as high frequencies such that we have a synchronous discharge of the VIII—nerve fibers along the length of the human cochlear partition, see Dau et al. (2000b) for details, and therefore, by temporal organization the response evoked by chirps should be larger than the one evoked by clicks.

In the left column in Fig. 3.2 it is noticeable that the latencies of the waves V corresponding to chirp stimulations have a larger separation among intensities than the latencies of the respective ABRs evoked by clicks. This last fact was related to the duration of the stimulus, as it can be seen in the right column where, after removing the offset of the chirps, the separation becomes smaller and is now *only* inherent to the response and not to the stimulus.

This study reinforced the results in Dau et al. (2000b); Fobel and Dau (2004) in the sense that chirps seem to be more appropriate at low stimulation levels for the detection of ABRs. In summary, the fibers of the VIII–nerve fire in a more synchronous way where evoked by a chirp than by a click, and the responses from these different areas of the BM contribute to have a higher final potential.

The results in Fig. 3.4 and 3.5 showed that the number of chirp stimulations to reach a significant discrimination of stimulation levels above the hearing threshold from the spontaneous activity is smaller than for click evoked ABRs with respect to the calibration described in Sec. 2.1.3 and the use of the GFPS as defined in Sec. 2.3.2. As consequence, the GFPS of chirp–evoked ABRs seems to be promising for the fast assessment of the integrity of the entire cochlea.

Use of Active Electrodes: At first sight, from the time domain average waveforms showed in Fig. 3.1, no difference can be seen regarding the type of electrodes. In addition, in Sec. 3.1.3, it was presented a comparison between passive and active electrodes, see Fig. 3.4 and 3.5 respectively, by showing the mean of $\overline{\Lambda}_1^I[1000]$ for the

spontaneous activity and increasing click and chirp intensities. The results showed that there is no clear tendency regarding the performance of the electrodes. However, active electrodes allow for an easier montage and are more robust to movements (Hagemann et al., 1985).

4.2.2   Gabor Frame Phase Stability

In this section of the work Gabor frame operators were introduced for the first time as analysis tool for ABRs. In earlier studies on chirp–evoked ABRs, a couple of thousands sweeps have been averaged and analyzed visually in the time domain (Dau et al., 2000b; Fobel and Dau, 2004). The presented approach here, is the first study that is directed to the fast single sweep processing of chirp–evoked ABRs.

In particular, this decomposition technique was used to derive the GFPS of sweep sequences of click and chirp–evoked ABRs. Analysis in the time domain, frequency domain and phase adjustment of ABRs were done and reported.

Specially, it is showed that ABRs as neural correlates of hearing allow for a reliable discrimination from the no–stimulation condition, i.e., spontaneous activity, with just a few hundreds of sweeps when using the GFPS as compared to conventional schemes in which thousands of sweeps had been averaged, see Sec. 1.2.

In fact, the GFPS showed to be an efficient feature extraction technique for ABR single sweep sequences that is in line, and can easily be included in the novelty detection paradigm using kernel machines as described in Sec.1.4 and in Corona-Strauss et al. (2007b) for a computational and truly automated hearing threshold detection.

Feature Extraction by Gabor Frame Operators: The amplitude of ABRs as natural large–scale measure of group synchronization at the brainstem level (see Rudell (1987) for an ABR generator model using volume conductor theory) can only be evaluated for large averages of sweeps due to a poor signal–to–noise ratio. As mentioned in Sec. 1.5, when comparing averaged evoked potentials to single sweeps, the amplitude information of the single sweeps results very fragile (Kolev and Yordanova, 1997), because the sweeps have a high degree of variance from one sweep to another, and therefore, even robust amplitude independent synchronization measures can not easily be applied to assess their synchronization stability. Note that the estimation of the

phase relation from experimental data represents an inverse problem in a mathematical sense. It has thoroughly been investigated in nonlinear dynamics, in particular for weakly coupled self–sustained chaotic oscillators, see Rosenblum et al. (2001) for a review. The reader is referred to Rosenblum et al. (2004) to see the role of phase locking in modern biosignal processing in a more general sense as presented here.

When the amplitude information is not considered and we focus purely on the phase, different approaches can be used instead, i.e., the wavelet phase coherence (Lachaux et al., 1999), which is mainly applied to measure the degree of phase locking of two signals in time, e.g., obtained from two different sites. This time–scale coherence measures take the non–stationary nature of evoked potentials into account.

Also, in contrast to the integral wavelet phase coherence, employed in Lachaux et al. (1999), Gabor frame operators can be sampled on less dense and thus less redundant time–frequency grids, see Fig. 2.4, and allow for an efficient analysis as well as synthesis. Consequently, they can be applied for the phase analysis of evoked response sequences as well as for the reconstruction of amplitude or phase modified/stabilized time domain waveforms, see Fig. 3.6. This is certainly an interesting concept not just for ABRs but for analyzing the phase reset in late evoked (cortical) potentials.

Note that the best results were obtained for lower frequency channels, i.e., $m = 1, 2$ (160–320 Hz and 320–480 Hz) which is line with the time–scale ABR entropy analysis in Strauss et al. (2004a), and also with the wavelet phase stability analysis performed in the study 2 as further discussed in Sec. 4.3.3. In particular we showed, as in Strauss et al. (2004a), that core information of ABRs is represented by low frequency components.

4.3 Study 2: Notched–Noise Embedded Frequency Specific Chirps

4.3.1 Stimuli

The notched–noise embedded frequency specific chirps, shown in Fig. 2.2, were developed to stimulate specific areas along the cochlear partition, and the advantage of a flat spectrum was to stimulate with the same intensity all the fibers of the auditory

nerve which are of interest. The fact that notched–noise was added to the stimulus, and that the chirps were calculated to start and end exactly with zero, was done to avoid stimulation of undesired areas of the cochlea due to an abrupt onset and offset of the stimulus. The study reported in Wegner and Dau (2002) obtained ABRs responses with a similar method like the one used in this work but only one low frequency chirp was tested and not a series that cover mostly the entire auditory range in humans.

It could be argued that an alternative approach using a broadband chirp combined with noise could limit the response to the bands of interest. Nevertheless, there are no results or comparisons for the approach presented here in which the following is accomplished: first, the stimuli are band limited and cover large proportion of the auditory range, and second, a notched–noise masking condition is added. The masking level used in this approach, was 20 dB below the pe SPL of the stimulations, as recommended in Stapells (1994) for low frequency specific brief tone–evoked ABRs. It can be further investigated which level of masking gives better results for low, medium, and high frequency specific chirp stimulations. And it could also be compared the effect of threshold estimations by using protocols with different masking noise, e.g., pink instead of white.

Also important to mention is that the latency–frequency function used to calculate the series of frequency specific chirps is based on the cochlear model of de Boer, which is considered as first order approximation of the behavior of the BM. Part of the further improvement could be to test the chirps constructed using a different approach on which the intensity factor is also included, such as the wave V latency curves reported by Gorga et al. (1988); Neely et al. (1988). These new family of chirps was developed and calibrated during this project, but the chirps based on the model of de Boer were preferred to be tested in the study 2, for details of this family of chirps see the Appendix B.

4.3.2   Auditory Brainstem Responses

In Fig. 3.7 the trace of the wave V for the different chirps can be extracted from the gray–scale map. Also in the same figure, the waves V (white lines) are easily identifiable for the different stimulation conditions, it can be seen how they are shifted in time when chirps with lower frequency content are applied.

From the last rows 5, 6 and 7, in Fig. 3.7, it can be seen that a realignment of waves

V still necessary (row 7) and therefore, the broadband chirp can still be improved. Theoretically if we would have responses evoked by "ideal" chirps, broadband, and band–limited, the sum of the waves V for the frequency specific chirps would not differ from the broadband response and realignment would not longer be necessary. The previously stated would mean that we manage to stimulate in a better and completely synchronized way the entire cochlea and the traveling wave delay for every frequency component is compensated.

In Fig. 3.8, the frequency–intensity relation of the latency of wave V, using the different stimuli, can be seen. For the highest intensity used in these experiments (50 dB pe SPL), the latencies are in general smaller as compared to the ones for lower intensities, such as 40 and 30 dB pe SPL. Likewise, the latency values for 40 dB pe SPL were smaller than the ones for 30 dB pe SPL. In the same figure and in Fig. 3.7 is noticeable the larger latencies corresponding to chirps stimulations with low frequency content (Ch1, Ch2) compared as to the smaller latencies of the responses for the chirps with higher frequency components (Ch3–Ch4). These results have a similar behavior as the latency curves reported in Neely et al. (1988), with the difference that instead of including a pure single frequency, they include a group of frequencies which covers in a large percentage the human auditory range.

The latency of the wave V is assumed to be a sum of a neural and a mechanical component. The mechanical component is sensitive to frequency and intensity of a stimulus, while the neural component can be assumed as constant (5 ms) (Neely et al., 1988; Dau et al., 2000b; Elberling et al., 2007). Note that the latencies plotted in Fig. 3.8 have a subtraction of 5 ms which corresponds to the neural component. This was done because the latency–frequency function, represented with a thick black line in the same figure, Fig. 3.8, is based on the model of de Boer which includes only the mechanical properties of the BM.

These results presented for the first time by frequency specific chirps demonstrated the fact that the tonotopic organization of the cochlea is related to the time that takes for a traveling wave to reach their sensation locus along the cochlear partition. We can conclude that we were able to extract frequency specific responses with the proposed method.

4.3.3   Wavelet Phase Stability

The motivation to analyze the WPS was to find out if the frequency channels, related to the scale a, used to analyze frequency specific chirp–evoked ABRs, would be different from the ones used in the analysis for broadband chirps by using GFPS, see Sec. 3.1.3 and also Corona-Strauss et al. (2008).

In Fig. 3.9 it can be seen that for all the conditions, the WPS is higher in the range of wave V and it becomes larger for the values of $a \geq 40$, where $a = 40$ corresponds to the frequency of 288 Hz. This is consistent to our previous findings reported in Sec. 3.1.3 and discussed in Sec. 4.2.2 (also published in Corona-Strauss et al. (2009)), where for GFPS analysis of chirp–evoked ABRs the channels with the highest energy of the ABRs corresponded to the frequency ranges of [160–230] and [320–480] Hz. In Fig. 3.9, for the B–bCh the WPS of the wave V is higher, even for the small values of a, which is supported by the fact that more fibers of the VIII–th nerve are stimulated.

The areas of higher WPS represented with light gray and white, becomes broader for large values of a. This also implies a loss in temporal resolution. Note that the temporal resolution decreases as a increases as consequence of Eq. 2.3.8. This is why is relevant to find an optimal value which results in a good compromise between temporal and frequency resolution, and $a=40$ seems to be a well supported choice. It can be concluded that the scale for the analysis of frequency specific chirp–evoked ABRs does not necessarily need to be different from the scale for broadband chirp–evoked ABRs, although this last ones can be analyzed using smaller values of a. Consequently the presented series of chirps can be used in the WPS scheme for the early HT detection in Corona-Strauss et al. (2007a).

4.4   Hybrid Detection Scheme

4.4.1   Adapted Filter Banks for Feature Extraction

The theory of signal–adapted filter banks has been developed in signal compression in recent years, e.g., see Moulin and Mihacak (1998) and references therein. Up to now, the underlying ideas mainly stick on this restricted area although they may have merit in other application fields such as pattern recognition. In recent papers, it has been

shown that an adaptation technique from signal compression is an effective tool for real world pattern recognition tasks when using appropriate class separability criteria, i.e., discrimination criteria instead of compression conditions, e.g., see Strauss et al. (2003) and references therein.

Here we used adapted filter banks to augment the phase synchronization approach by morphological features located in time and frequency. In particular, we have introduced adapted filter banks for the construction of sphere in kernel feature spaces induced by reproducing kernels of kernel learning machines. These feature vectors are extracted in a way that they include a priori information about the pattern recognition at hand task, i.e., latency jitters, as well as the kernel based novelty detection machine used.

These morphological time–frequency information makes the analysis more robust as the final decision making is not exclusively based on one type of feature, i.e., the instantaneous phase.

Note that the used lattice structure implementation of filter banks allows for a very efficient implementation, e.g., see Vaidyanathan and Hoang (1988), even in the used nonsubsampled version. We used this nonsubsampled implementation as it is truly shift–invariant such that the feature vector is invariant to latency jitters.

This nonsubsampled implementation which results in a tight frame decomposition procedure is also known as "algorithm a trous" (Shensa, 1992) and is equivalent to the so–called "cyclic spinning" (Coifman and Donoho, 1995). There exist nearly shift–invariant approaches with lower arithmetic complexity, e.g., see Kingsbury (2001). However, we stuck to the completely shift–invariant approach which can efficiently be implemented for the used filters of order 5. Nevertheless, comparing our scheme to these approximate shift–invariant approaches regarding the performance as well as using more flexible parameterizations of filter banks, e.g., see Daubechies and Sweldens (1998) might be an interesting point of further research.

4.4.2 Kernel Based Novelty Detection of ABRs

We have presented a hybrid ABR detection scheme using the Gabor frame phase stability combined with kernel based novelty detection machines. This was the first time that these machines have been applied to detect synchronized activity as novel instance.

In Strauss et al. (2004b) a kernel based novelty detection approach has been introduced for the ABR detection. However, in Strauss et al. (2004b) the sphere in the feature space was constructed by using physiological data for stimulations above the hearing threshold in order to discriminate it from the spontaneous activity and not to detected synchronized activity as novel instance. The latter has the following advantages: the sweeps of the spontaneous activity are considered as standard or learned class in a machine learning context and the synchronized activity at the brainstem level is detected as novel instance. Since such a system is trained with the spontaneous activity, it is adjusted to the measurement conditions on site and thus robust to non–stimulus locked artifacts, e.g., related the technical infrastructure and electrode placement.

Based on our previous results regarding the stimulus/stimulation intensity and the electrodes, we used a fixed chirp stimulation intensity of 30 dB pe SPL and active electrodes to implement this scheme. With just 200 sweeps, we achieved a detection of the stimulation almost in all the subjects. However, this study represents just a first trail of combining phase synchronization features with morphological time–frequency information. The results are promising, however, further work should be related to a direct integration of phase related features in kernel machines such as using the GFPS for several samples and deliver them as higher dimensional feature vector to the kernel machine. Of course, these approaches might require a lot of engineering heuristics, e.g., finding the optimal number of features.

4.5   Future Work and Limitations

More clinically oriented studies are necessary to evaluate the real value of the presented analysis for fast hearing threshold detection systems. The presented method is related to the feature extraction stage of conjoint detections systems and thus just provides a signal analytic basis for such studies. We have also implemented the combination of phase synchronization feature extraction with a hybrid adapted filter bank – kernel machine scheme which provided an excellent performance. However future research should analyze this combination more carefully, especially regarding the direct integration of phase related features in the novelty detection system. Also important will be to test the presented scheme using ABR data collected from newborns.

Future analysis can be done to make a faster recognition of frequency specific chirp–

evoked ABRs. Also interesting will be to evaluate the notched–noise embedded chirps with patients with different types of hearing loss, and make a comparison against the commonly accepted methods. A comparison between different levels of masking noise, as mentioned in Sec. 4.3.1 and their effects can also be further investigated, such as finding the best masking intensity for specific frequency bands, using different type of noise, and comparing the results against general accepted threshold estimation methods reported in literature.

As already mentioned in Sec. 4.3.1, the model used to calculate the series of chirps is considered as a first approximation of the behavior of the BM. We consider that in addition, improvements related to the stimuli can be done by making the chirps intensity specific, using e.g, the latency plots reported in Neely et al. (1988). See in the Appendix B an example of such implementation. Further evaluation in subjects can be done with these new stimuli, and also a comparison against the already tested chirps based on the de Boer model.

Chapter 5

Conclusions

We have presented a new approach for the fast detection of wave V in ABRs using smart single analysis systems which are based on a novelty detection paradigm.

In this work, different time–frequency analysis transformations, CWT and GFs, were used to evaluate phase synchronization features of ABRs. GFs were introduced as novel feature extraction method to derive the GFPS of ABR single sweep sequences. This method provided a discrimination of the spontaneous activity from stimulations above the HT with a minimum number of sweeps. It is concluded that the GFPS analysis represents a robust feature for ABR single sweep sequences.

We conclude that our studies reinforced the use of optimized chirp stimulations for the fast hearing threshold detection, especially at low stimulus intensities.

There was no clear tendency regarding the electrodes. However, considering the fact that active electrodes allow for an easier montage and are more robust to movements, they seemed to be preferable for our purpose.

We also presented the development and testing of a series of notched–noise embedded frequency specific chirps, which allowed the assessment of frequency specific ABRs with an identifiable wave V for different intensity levels. The resultant wave V latency measures showed a similar behavior as for the latency–frequency functions reported in literature. The WPS of frequency specific chirp–evoked ABRs reflected the presence of the wave V for all stimulation intensities. The scales that resulted in higher WPS are in line with previous findings, where ABRs evoked by broadband chirps were analyzed, which stated that low frequency channels are better for the recognition and analysis of chirp–evoked ABRs.

It is finally concluded that the proposed novelty detection paradigm, including the new signal processing procedures and stimulation techniques, improves the detection of ABRs in terms of the degree of objectivity, i.e., automation of procedure, and measurement time. It represents therefore a promising approach to improve the effectiveness of NHS programs. However, the proposed schemes have to be evaluated in further, more clinically oriented studies.

Appendix A

Lattice Parametrization of Paraunitary Filter Banks

Let $G_0(z)$ and $G_1(z)$ be the synthesis filters of a normalized paraunitary two–channel FIR filter bank with real filter coefficients and a zero mean high–pass. When cascading such a two–channel building block in an octave–band tree, the filters of an equivalent parallel structure are given by

$$Q_{j,0}(z) = \prod_{m=0}^{j-1} G_0(z^{2^m}) \tag{App. 1}$$

and

$$Q_{j,1}(z) = G_1(z^{2^{j-1}}) \prod_{m=0}^{j-2} G_0(z^{2^m}). \tag{App. 2}$$

Let us denote the translations of the impulse responses $q_{j,k}[\cdot]$ of these filters by $\mathbf{q}_{j,i}^m = (q_{j,i}[k - 2^j m])_{k \in \mathbb{Z}}$ $(i = 0, 1)$ and let J be the maximal decomposition depth. Then the set

$$\left\{ \mathbf{q}_{J,0}^m, \mathbf{q}_{j,1}^m \; : \; j = 1, \ldots, J; m \in \mathbb{Z} \right\} \tag{App. 3}$$

constitutes an orthonormal basis for ℓ^2 and an arbitrary sequence $\mathbf{x} \in \ell^2$ can be decomposed as

$$\mathbf{x} = \sum_{m \in \mathbb{Z}} d_{J,0}[m] \, \mathbf{q}_{J,0}^m + \sum_{j=1}^{J} \sum_{m \in \mathbb{Z}} d_{j,1}[m] \mathbf{q}_{j,1}^m.$$

We denote the *wavelet coefficients* by $\mathbf{d}_j = (d_{j,1}[m])_{m \in \mathbb{Z}}$.

All paraunitary filter banks can be parameterized by the lattice structure Vaidyanathan (1993), where the polyphase matrix of the analysis bank $\mathbf{H}_{\mathrm{pol}}(z)$ as a decomposition

of the form

$$\mathbf{H}_{\text{pol}}(z) = (\prod_{l=0}^{L-1} \begin{pmatrix} \cos\vartheta_l & \sin\vartheta_l \\ -\sin\vartheta_l & \cos\vartheta_l \end{pmatrix} \begin{pmatrix} 1 & 0 \\ 0 & z^{-1} \end{pmatrix}) \begin{pmatrix} \cos\vartheta_L & \sin\vartheta_L \\ -\sin\vartheta_L & \cos\vartheta_L \end{pmatrix}, \quad \text{(App. 4)}$$

where $\vartheta_L \in [0, 2\pi)$ and $\vartheta_l \in [0, \pi)$ $(l = 0, \ldots, L-1)$. Let ϑ_L be the residue of $\frac{\pi}{4} - \sum_{l=0}^{L-1} \vartheta_l$ modulo 2π in $[0, 2\pi)$. Then the space

$$\mathcal{P}^L := \{\boldsymbol{\vartheta} = (\vartheta_0, \ldots, \vartheta_{L-1}) : \vartheta_l \in [0, \pi)\}$$

can serve to parameterize all two–channel paraunitary filter banks with at least one vanishing moment of the high–pass filter, see Strauss and Steidl (2002) for more detailed discussions. To emphasize this parametrization we will use the superscript $\boldsymbol{\vartheta}$ later.

The orthogonal decomposition described above is very efficient in its implementation as it based on maximally decimated filter banks. However, such orthogonal decompositions are strongly shift–variant Simoncelli et al. (1992); Vetterli and Kovačević (1995) and a minimal shift of the signal to be analyzed results in a significant redistribution of the energy induced in the individual octave bands Simoncelli et al. (1992).

Due to the biological origin of ABRs, we expect inter–sweep latency differences. In other words, the discriminant information in ABRs separating sweeps of the spontaneous activity from stimulations above the hearing threshold is unlikely to occur with the very same latency for all the sweeps.

To overcome this problem, we replace the shift–variant orthonormal wavelet basis (App. 3) by the tight wavelet frame

$$\{2^{-J/2}\tilde{\mathbf{q}}_{J,0}^m, 2^{-j/2}\tilde{\mathbf{q}}_{j,1}^m : j = 1, \ldots, J; m \in \mathbb{Z}\},$$

where $\tilde{\mathbf{q}}_{j,i}^m := (q_{j,i}[k - m])_{k \in \mathbb{Z}}$ $(i = 0, 1)$. Then $\mathbf{x} \in \ell^2$ can be decomposed as

$$\mathbf{x} = \sum_{m \in \mathbb{Z}} \tilde{d}_{J,0}[m]\, \tilde{\mathbf{q}}_{J,0}^m + \sum_{j=1}^{J} \sum_{m \in \mathbb{Z}} \tilde{d}_{j,1}[m]\tilde{\mathbf{q}}_{j,1}^m \quad \text{(App. 5)}$$

with the coefficients

$$\tilde{d}_{j,i}[m] = \frac{1}{2^j}\langle \mathbf{x}, \tilde{\mathbf{q}}_{j,i}^m\rangle_{\ell^2} \quad (i = 0, 1).$$

We set

$$\tilde{\mathbf{d}}_j := \left(\tilde{d}_{j,1}[m]\right)_{m \in \mathbb{Z}} \quad (j = 1, \ldots, J).$$

Overcomplete expansions can be implemented by oversampled paraunitary filter banks Cvetković and Vetterli (1998); Bölcskei et al. (1998). The highly redundant expansion (App. 5) corresponds to a nonsubsampled filter bank, i.e., we have no multirate operations at all. In this special case, the subbands are obtained by pure linear time–invariant (LTI) filters related to Eq. (App. 1) and (App. 2), respectively.

Although nearly shift–invariant approaches with lower arithmetic complexity, might also be an option, e.g., see Kingsbury (2001), see stick to the completely shift–invariant implementation as they can easily be implemented in real–time for the application considered here and the used filters of order 5.

Feature Spaces Induced by Reproducing Kernels

Let $K : \mathcal{X} \times \mathcal{X} \longrightarrow \mathbb{R}$ ($\mathcal{X}$ is a compact subset of $\mathbb{R}^d$) be a positive definite symmetric function in $L^2(\mathcal{X} \times \mathcal{X})$. For a given K, there exists a *reproducing kernel Hilbert space*

$$\mathcal{H}_K = \overline{\text{span}\left\{K(\tilde{\mathbf{x}}, \cdot) : \tilde{\mathbf{x}} \in \mathcal{X}\right\}}$$

of real valued functions on $\mathcal{X}$ with inner product determined by

$$\langle K(\tilde{\mathbf{x}}, \mathbf{x}), K(\bar{\mathbf{x}}, \mathbf{x})\rangle_{\mathcal{H}_K} = K(\tilde{\mathbf{x}}, \bar{\mathbf{x}})$$

which has the reproducing kernel K, i.e., $\langle f(\cdot), K(\tilde{\mathbf{x}}, \cdot)\rangle_{\mathcal{H}_K} = f(\tilde{\mathbf{x}})$ ($f \in \mathcal{H}_K$). By *Mercer's Theorem*, the reproducing kernel K can be expanded in a uniformly convergent series on $\mathcal{X} \times \mathcal{X}$

$$K(\mathbf{x}, \mathbf{y}) = \sum_{j=1}^{\infty} \eta_j \varphi_j(\mathbf{x}) \varphi_j(\mathbf{y}), \tag{App. 6}$$

where $\eta_j \geq 0$ are the eigenvalues of the integral operator $T_K : L^2(\mathcal{X}) \to L^2(\mathcal{X})$ with

$$T_K f(\mathbf{y}) = \int_{\mathcal{X}} K(\mathbf{x}, \mathbf{y}) f(\mathbf{x}) \, \mathrm{d}\mathbf{x}$$

and where $\{\varphi_j\}_{j \in \mathbb{N}}$ are the corresponding $L^2(\mathcal{X})$–orthonormalized eigenfunctions. We restrict our interest to functions K that arise from a radial basis function (RBF). In other words, we assume that there exists a real valued function k on $\mathbb{R}$ so that

$$K(\mathbf{x}, \mathbf{y}) = k(||\mathbf{x} - \mathbf{y}||_2), \tag{App. 7}$$

where $|| \cdot ||_2$ denotes the Euclidean norm on $\mathbb{R}^d$.

We introduce a so–called *feature map* $\boldsymbol{\Phi} : \mathcal{X} \to \ell^2$ by

$$\boldsymbol{\Phi}(\cdot) = \left(\sqrt{\eta_j}\varphi_j(\cdot)\right)_{j \in \mathbb{N}}.$$

Let ℓ^2 denote the Hilbert space of real valued quadratic summable sequences $a = (a_i)_{i \in \mathbb{N}}$ with inner product $\langle a, b \rangle_{\ell^2} = \sum_{i \in \mathbb{N}} a_i b_i$. By (App. 6), we have that $\boldsymbol{\Phi}(\mathbf{x})$ ($\mathbf{x} \in \mathcal{X}$) is an element in ℓ^2 with

$$||\boldsymbol{\Phi}(\mathbf{x})||_{\ell^2}^2 = \sum_{j=1}^{\infty} \eta_j \varphi_j^2(\mathbf{x}) = K(\mathbf{x}, \mathbf{x}) = k(0).$$

We define the *feature space* $\mathcal{F}_K \subset \ell^2$ by the ℓ^2–closure of all finite linear combinations of elements $\boldsymbol{\Phi}(\mathbf{x})$ ($\mathbf{x} \in \mathcal{X}$)

$$\mathcal{F}_K = \overline{\operatorname{span}\{\boldsymbol{\Phi}(\mathbf{x}) : \mathbf{x} \in \mathcal{X}\}}.$$

Then $\mathcal{F}_K$ is a Hilbert space with $|| \cdot ||_{\mathcal{F}_K} = || \cdot ||_{\ell^2}$. The feature space $\mathcal{F}_K$ and the reproducing kernel Hilbert space $\mathcal{H}_K$ are isometrically isomorph with isometry $\iota : \mathcal{F}_K \to \mathcal{H}_K$ defined by $\iota(\mathbf{w}) = f_{\mathbf{w}}(\mathbf{x}) = \langle \mathbf{w}, \boldsymbol{\Phi}(\mathbf{x}) \rangle_{\ell^2} = \sum_{j=1}^{\infty} w_j \sqrt{\eta_j}\varphi_j(\mathbf{x})$.

Appendix B

Family of series of Notched–noise embedded frequency specific Chirps using ABR-latency frequency functions

In the main work was presented a series of chirps developed for the detection of frequency specific ABR responses, see Sec. 2.1.2. That series of chirps was calculated using as latency–frequency function the mechanical model of de Boer.

In this section is described the generation of a family of series of frequency specific chirps, which was also developed and calibrated during this project. This new family or set of series was based on the latency–frequency functions reported by Neely and colleagues in Neely et al. (1988), see Fig. App. 1. These functions were approximated from experimental tone evoked–ABR data. This set of chirps have the advantage of not only compensate for the dispersion of the basilar membrane but also to be intensity level specific. Thus, a series of chirps was created for the intensity levels of 20, 30 and 40 dB SPL, respectively. The calculation procedure was similar as the one described in Sec. 2.1.1, and Sec. 2.1.2.

A brief summary of the methodology is given here. First, the latency–frequency function was based on the equation which represents the ABR wave V latency as reported in Neely et al. (1988):

$$\tau_{\mathrm{BM}}(f) = a + bc^{-i}f^{-d} \qquad\qquad (\text{App. 8})$$

with $a = 5.0$ ms, $b = 12.9$ ms, $c = 5.0$, $d = 0.413$, with i representing the stimulus intensity (in dB SPL divided by 100) and f representing the stimulus frequency divided by 1 kHz, the different bands were calculated using a range of 10400 Hz and the central
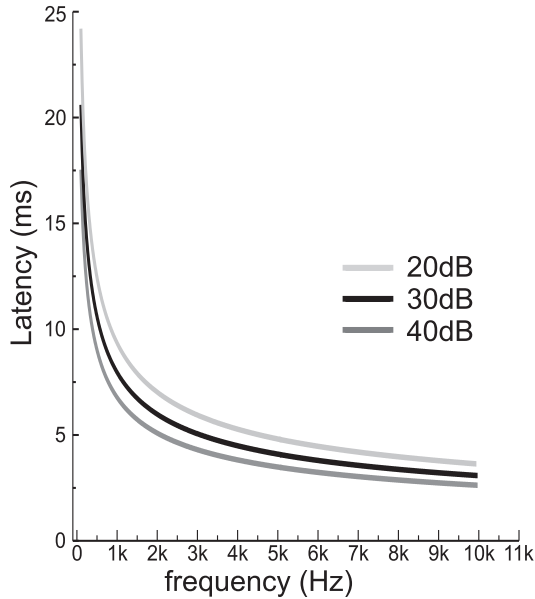
Figure App. 1: Latency–frequency functions developed by Nelly and colleagues, based on experimental tone evoked–ABR data. The functions are shown for different intensity levels. The light gray line corresponds to the intensity level of 20 dB SPL, the black line to 30 dB SPL and the dark gray line to 40 dB SPL. Note that these latency values include the neural and mechanical component, as they are reported directly from experimental data, and not just the mechanical component as for the case of the series of chirps developed using the mechanical model of de Boer.

frequencies and ranges as described in Tab. App.1 (original values). The frequency bands were identical for all intensity levels.

As explained in Sec. 2.1.1, τ_{BM} was considered a representation of the propagation time, and therefore the inverse function of τ_{BM} was calculated, that is $\tau_{\mathrm{BM}}^{-1}(f)=f_a(t)$, where $t=\frac{1}{f}$. The next step was to calculate the chirps using the corresponding frequency bands and the same equations as in Sec. 2.1.1, Eq.(2.1.2), (2.1.3), and (2.1.4).

The initial resultant chirps not always had zero values at their beginning and at their end, and therefore, the original calculated ranges had to be modified in order to accomplish this condition; as well as fulfill the requirement of having at least "3–half–waves".

The final intervals, central frequencies and durations of all the chirps are also shown in Tab. App.1. The resultant waveforms for the three sets of chirps are shown in the Fig. App. 2. For identification purpose, the chirps are called Ch1, Ch2, Ch3, Ch4, and

Table App. 1: Original (calculated) and final parameters of the family of series of frequency specific chirps using latency–frequency functions, for the intensity levels of 40, 30 and 20 dB SPL. Where range is 10400 Hz, BW is bandwidth, and fc is central frequency.

Parameter	Ch1	Ch2	Ch3	Ch4	Ch5	B-bCh
Original Range	range/$2^5 \equiv 312.5$	range/$2^4 \equiv 625$	range/$2^3 \equiv 1250$	range/$2^2 \equiv 2500$	range/$2^1 \equiv 5000$	range/$2^0 \equiv 9900$
40 dB BW (Hz)	290	625	1200	2505	5046.5	9899.5
30 dB BW (Hz)	324	660	1220	2420	5140	4900
20 dB BW (Hz)	284	680	1210	2530	4560	9900
Original fc (Hz)	250	750	2000	4000	8000	5050
40 dB fc (Hz)	250	750	2000	4007.5	8002.5	5049.75
30 dB fc (Hz)	250	750	2000	4000	8000	5050
20 dB fc (Hz)	250	750	2000	4000	8000	5050
Original Interval (Hz)	[93.75, 406.25]	[437.5, 1062.5]	[1375, 2625]	[2750, 5250]	[5500, 10500]	[100, 10000]
40 dB Interval (Hz)	[105, 395]	[437.5, 1062.5]	[1400, 2600]	[2755, 5260]	[5477, 10523.5]	[100, 9999.5]
30 dB Interval (Hz)	[88, 412]	[420, 1080]	[1390, 2610]	[2790, 5210]	[5430, 10570]	[100, 9999.5]
20 dB Interval (Hz)	[108, 392]	[410, 1090]	[1395, 2605]	[2735, 5265]	[5720, 10280]	[100, 10000]
40 dB duration (ms)	7.244	2.925	1.330	1.045	0.794	14.921
30 dB duration (ms)	10.238	3.679	1.592	1.185	0.952	17.526
20 dB duration (ms)	9.677	4.489	1.853	1.462	0.978	20.587

Ch5 according to their frequency range, where Ch1 is for the stimulus with the lowest frequency band and Ch5 is for the chirp with the highest frequency band.

In the Fig. App. 3 is shown the generation procedure of the chirps for the different bands for the intensity level of 20 dB SPL. The chirps are also directly related to the latency–frequency function. In Fig. App. 4 and Fig. App. 5 are shown the same information for the chirps at the intensity levels of 30 and 40 dB SPL, respectively. In these figures is easy to extract the different frequency bands and the respective durations of the chirps, which are directly related to the intensity level at which they were calculated.

The effect of the zero correction can be seen more in some of the chirps, i.e., Ch1 at 30 dB SPL, which lowest frequency moved from 93.75 to 88 Hz. This family of chirps could be evaluated in a future research, and could be compared against the chirps constructed based on the mechanical model of de Boer.

A noise file was also created, as described for the chirps in Sec. 2.1.2, which fitted the frequency bands of each chirp developed.

The calibration of this set of stimuli was achieved following the same procedure as the one reported in Sec. 2.1.3, by obtaining the pe SPL of each chirp.
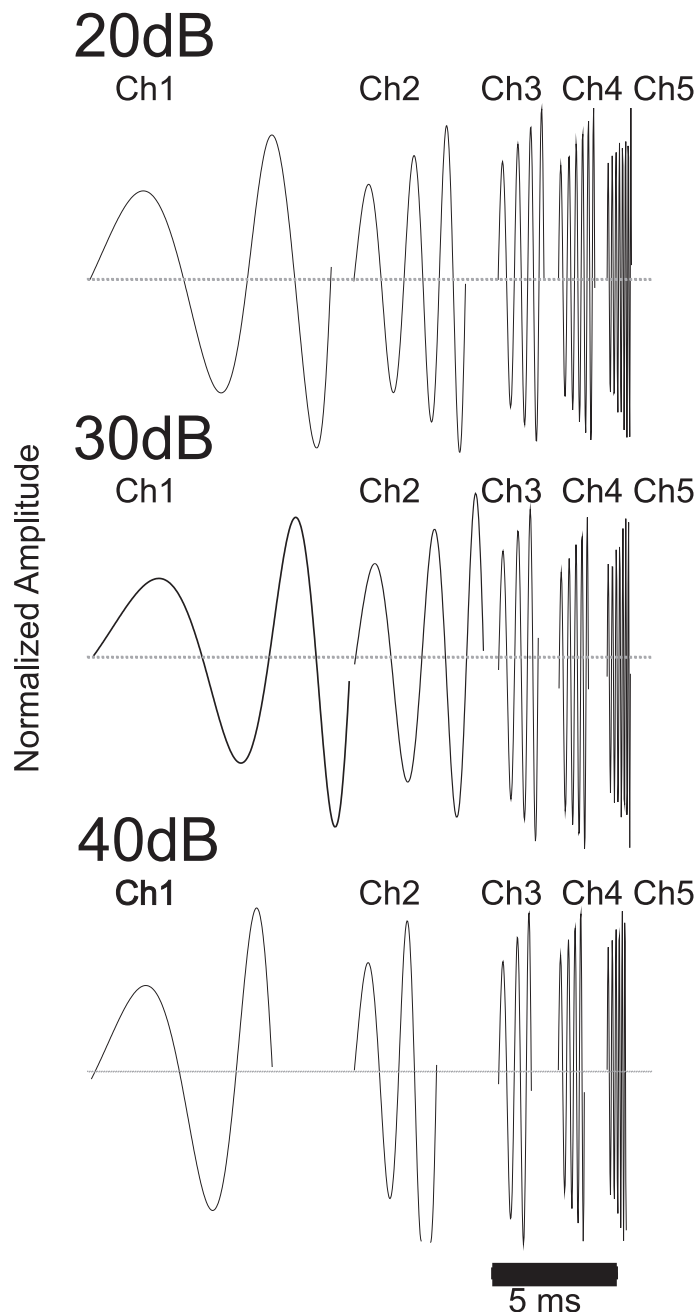
Figure App. 2: Resultant waveforms of the series of frequency specific chirps for the different intensity levels. The chirps are called Ch1, Ch2, Ch3, Ch4, and Ch5 according to their frequency range, where Ch1s are the stimuli with the lowest frequency band and Ch5s are for the chirp with the highest frequency band. From top to bottom, series of chirps for the intensity level of 20, 30 and 40 dB SPL, respectively. Note the longer durations of the chirps for the intensity levels of 20 dB SPL with regard to the chirps at 30 and 40 dB SPL, and at the same time the longer durations of the chirps at 30 dB SPL with regard to the chirps at 40 dB SPL, respectively.
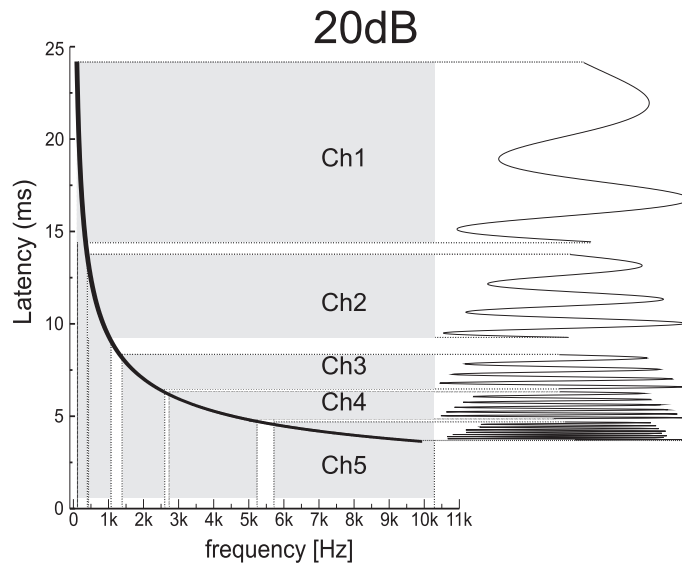
Figure App. 3: Generation sketch of the series of band limited chirps using the latency–frequency function based on fitted ABR latency curves, as reported in Neely et al. (1988), for the intensity level of 20 dB SPL.
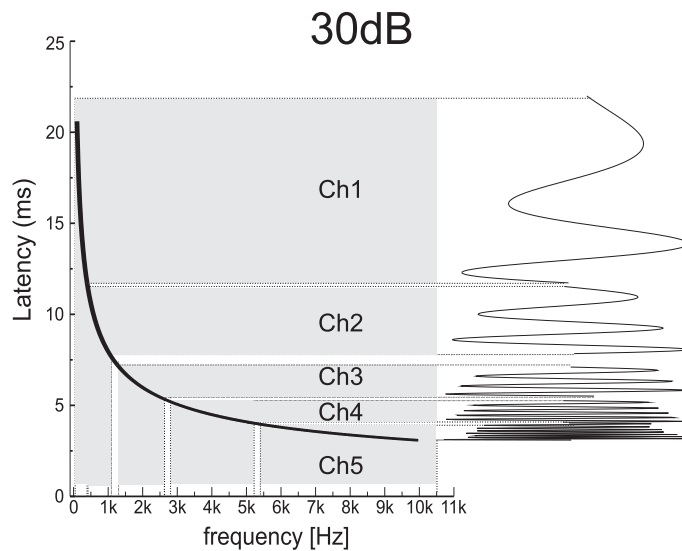
Figure App. 4: Generation sketch of the series of band limited chirps using the latency–frequency function based on fitted ABR latency curves, as reported in Neely et al. (1988), for the intensity level of 30 dB SPL.
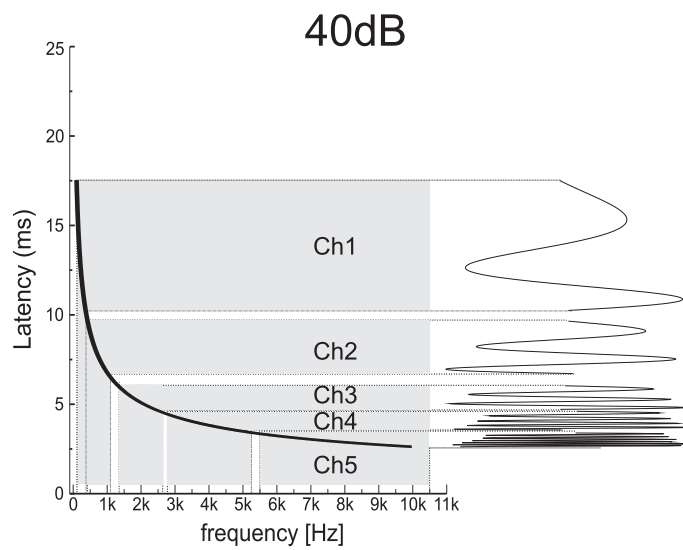
Figure App. 5: Generation sketch of the series of band limited chirps using the latency–frequency function based on fitted ABR latency curves, as reported in Neely et al. (1988), for the intensity level of 40 dB SPL.

Bibliography

P. Abry. *Ondelettes et turbulence. Multirésolutions, algorithmes de décomposition, invariance d'échelles.* Diderot Editeur, Paris, 1997.

N. Acir, O. Ozdamar, and C. Guzelis. Automatic classification of auditory brainstem responses using svm-based feature selection algorithm for threshold detection. *Engr. App. Artif. Intel.*, 2006. In press.

M. Akay. *Time Frequency and Wavelets in Biomedical Signal Processing.* Wiley, NY, 1997.

D. Alpsan, M. Towsey, Ö. Özdamar, A. Tsoi, and G. N. Ghista. Determining hearing threshold from brain stem evoked potentials. *IEEE Eng. Med. Biol. Mag.*, 13:465–471, 1994.

A. Ben-Hur, D. Horn, H. T. Siegelman, and V. Vapnik. Support vector clustering. *Journal of Machine Learning Research*, pages 125–137, 2001.

H. Bölcskei, F. Hlawatsch, and H. G. Feichtinger. Frame-theoretic analysis of oversampled filter banks. *IEEE Trans. Signal Processing*, 46:3256–3268, 1998.

A. Bruns. Fourier–, hilbert–, and wavelet based signal analysis: are they really different approaches ? *J. of Neuroscience Methods*, 137:321–332, 2004.

R. M. Burkard, M. Don, and E. J. J. *Auditory Evoked Potentials: Basic Principles and Clinical Application.* Lippincott Williams & Wilkins, 2006.

S. J. Chen, E. Y. Yang, M. L. Kwan, P. Chang, A. S. Shiao, and C. F. Lien. Infant hearing screening with an automated auditory brainstem response screener and the auditory brainstem response. *Acta. Paediatr.*, 85:14–18, 1996.

R. R. Coifman and D. Donoho. Translation invariant de–noising. In A. Antoniadis, editor, *Wavelet in Statistics*, Lecture Notes, Springer Verlag, pages 125–150, New York, 1995.

R. R. Coifman and M. V. Wickerhauser. Entropy based algorithms for best basis selection. *IEEE. Trans. on Information Theory*, 32:712–718, 1992.

F. I. Corona-Strauss, W. Delb, M. Bloching, and D. J. Strauss. Ultra–fast quantification of hearing loss by neural synchronization stabilities of auditory evoked brainstem activity. In *In Proceedings of the 29th Conference of the IEEE Engineering in Medicine and Biology Society*, pages 2476–2479, Lyon, France, 2007a.

F. I. Corona-Strauss, W. Delb, B. Schick, and D. J. Strauss. On the single sweep processing of auditory brainstem responses: click vs. chirp stimulations and active vs. passive electrodes. In *Conf Proc IEEE Eng Med Biol Soc*, volume 2008:1, pages 4166–4169, 2008.

F. I. Corona-Strauss, W. Delb, B. Schick, and D. J. Strauss. Phase stability analysis of chirp evoked auditory brainstem responses by gabor frame operators. *IEEE Trans Neural Syst Rehabil Eng. accepted*, 2009.

F. I. Corona-Strauss, D. J. Hecker, W. Delb, and D. J. Strauss. Ultra–fast detection of hearing thresholds by single sweeps of auditory brainstem responses: A new novelty detection paradigm. In *Conf Proc IEEE Eng Med Biol Soc*, pages 638–641, Kohala Coast, HI, USA, 2007b.

M. T. Cover and J. A. Thomas. *Elements of Information Theory*. Wiley, NY, 1991.

Z. Cvetković and M. Vetterli. Oversampled filter banks. *IEEE Trans. on Signal Processing*, 46:1245–1255, 1998.

T. Dau, O. Wegner, V. Mellert, and B. Kollmeier. Auditory brainstem responses (ABR) with optimized chirp signals compensating basilar-membrane dispersion. *J. Acoustical Soc. Am.*, 107:1530–1540, 2000a.

T. Dau, O. Wegner, V. Mellert, and B. Kollmeier. Auditory brainstem responses with optimized chirp signals compensating basilar–membrane dispersion. *J. Acoust. Soc. Am.*, 107:1530–1540, 2000b.

I. Daubechies. *Ten Lectures on Wavelets*. SIAM, Philadelphia, PA, 1992.

I. Daubechies and W. Sweldens. Factoring wavelet transforms into lifting steps. *J. Fourier Anal. Appl.*, 4(3):245–267, 1998.

A. G. de Aledo Linos. Programa de detectión precoz de la hipoacusia infantil en cantabria. *Bol. Pediatrics*, 41:54–61, 2001.

E. de Boer. Auditory physics. physical principles in hearing theory I. *Phys. Rep.*, 62:87–174, 1980.

W. Delb. Universal neonatal hearing screening in germany. what is the next step? *HNO*, 50:607–610, 2002.

W. Delb. Universal neonatal screening as an application of automated audiological techniques. *HNO*, 51:962–965, 2003.

W. Delb, R. D'Amelio, O. Schonecke, and H. Iro. Are there psychological or audiological parameters determining the tinnitus impact. In J. W. P. Hazell, editor, *Proceedings of the 6th tinnitus seminar*, pages 446–451, Cambridge, UK, 1999. Oxford University Press.

W. Delb, D. Merkel, K. Pilorget, J. Schmitt, and P. K. Plinkert. Effectiveness of a teoae-based screening program. can a patient-tracking system effectively be organized using modern information technology and central data management? *Eur. Arch. Otorhinolaryngol.*, 261:191–196, 2004.

R. E. Delgado, Ö. Özdamar, and E. Miskiel. On–line system for automated auditory evoked response threshold determination. In *Proceedings of the 11th Silver Anniversary International Conference of the IEEE Engineering in Medicine and Biology Society*, pages 1472–1473, 1988.

R. A. Dobie and M. J. Wilson. Analysis of auditory evoked potentials by magnitude-squared coherence. *Ear & Hearing*, 10:2–13, 1989.

M. Don, B. Kwong, C. Tanaka, D. Brackmann, and N. R. The stacked abr: A sensitive and specific tool fpr detecting small acoustic tumors. *Audiology Neurotology*, 10:271–290, 2005.

M. Don, A. Masuda, R. Nelson, and D. Brackmann. Succesful detection of small acoustic tumors using the stacked derived-band auditory brain stem response amplitude. *The American Journal of Otology*, 18:608–621, 1997.

C. Elberling, M. Don, M. Cebulla, and E. Stürzebecher. Auditory steady-state responses to chirp stimuli based on cochlear traveling wave delay. *Journal of the Acoustical Society of America*, 122:2772–2785, 2007.

European Committe for Standardization. Electroacustics- audiometric equipment. part 3: Test signals of short duration. Technical Report, The European Standard. EN 60645-3:2007., 2007.

O. Fobel and T. Dau. Searching for the optimal stimulus eliciting auditory brainstem responses in humans. *J. Acoustical Soc. Am.*, 116:2213–2222, 2004.

G. G. Gentiletti-Faenze, O. Yanez-Suarez, and J. M. Cornejo. Evaluation of automatic identification algorithms for auditory brainstem response used in universal hearing loss screening. In *Proceedings of the 25th International Conference of the IEEE Engineering in Medicine and Biology Society*, pages 2857–2860, Cancun, Mexico, 2003.

P. Gorga, J. R. Kaminski, K. A. Beauchaine, and W. Jesteadt. Auditory brainstem responses to tone-bursts in normally hearing subjects. 31:87–97, 1988. J. Speech Hear. Res.

P. Goupillaud, A. Grossmann, and J. Morlet. Cycle–octave and related transforms in seismic signal analysis. *Geoexploration*, 23:85–102, 1984.

D. D. Greenwood. A cochlear frequency-position function for several species–29 years later. *J Acoust Soc Am.*, 87:2592–2605, 1990.

B. Hagemann, G. Luhede, and H. Luczak. Improved "active" electrodes for recording bioelectric signals in work physiology. *European Journal of Applied Physiology*, 54: 95–98, 1985.

J. W. Hall. *Handbook of Auditory Evoked Responses.* Allyn and Bacon, Needham Heights, MA, 1992.

M. Helfand, D. C. Thompson, R. Davis, H. McPhillips, C. J. Homer, and S. Lieu, T.Sivalal. Newborn hearing screening, systematic evidence review number 5. AHRQ Publication No 02-S001, Rockville MD Agency for Healthcare Research and Quality, 2001.

International Organization for Standarization. Acoustics - reference zero for the calibration of audiometric equipment. part 6: Reference threshold of hearing for test signals of short duration. Technical Report, International Standards for Business. ISO 389-6:2007., 2007.

N. G. Kingsbury. Complex wavelets for shift invariant analysis and filtering of signals. *J. of Applied Computation and Harmonic Analysis*, 10:234–253, 2001.

K. Kodera, Yamane, H. Yamada, and O. S. JI. The effect of onset, offset and rise-decay times of tone bursts on brain stem response. *Scand Audiol.*, 6:205–210, 1977.

A. Kolev and J. Yordanova. Analysis of phase–locking is informative for studying event–related potentials. *Biological Cybernetics*, 76:229–235, 1997.

J.-P. Lachaux, E. Rodriguez, J. Martinerie, and F. J. Varela. Measuring the phase synchrony in brain signals. *Human Brain Mapping*, 8:194–208, 1999.

A. K. Louis, P. Maass, and A. Rieder. *Wavelets: Theory and Application.* John Wiley & Sons, Baffins Lane, Chichester, West Sussex, 1997.

Y. F. Low, F. I. Corona-Strauss, P. Adam, and D. J. Strauss. Extraction of auditory attention correlates in single sweeps of cortical potentials by maximum entropy paradigms and its application. In *Proceedings of the 3st Int. IEEE EMBS Conference on Neural Engineering*, pages 469–472, Kohala Coast, HI, USA, 2007.

H. Luts and J. Wouters. Hearing assessment by recording multiple auditory steady–state responses: the influence of test duration. *International Journal of Audiology*, 43:471–478, 2004.

G. P. Madhavan, D. B. H., A. R. M. Upton, and M. E. Jernigan. Classification of brainstem auditory evoked potentials by syntactic methods. *Electroenceph. Clin. Neurophysiol.*, 65:289–296, 1986.

M. Markou and S. Singh. Novelty detection: A review, part I: Statistical approaches. *Signal Processing*, 83:2481—2498, 2003a.

M. Markou and S. Singh. Novelty detection: A review, part II: Neural network based approaches. *Signal Processing*, 83:2499—2521, 2003b.

S. M. Mason and W. Adams. An automated microcomputer based electric response audiometry system for machine scoring of auditory potentials. *Clin. Phys. Physiol. Meas.*, 5:219–222, 1984.

S. Meier, O. Narabayashi, R. Probst, and N. Schmuzinger. Comparison of currently available devices designed for newborn hearing screening using automated auditory brainstem and/or otoacoustic measurements. *Int. J. Pediatr. Otorhinolaryngol.*, 68: 927–937, 2004.

P. Moulin and K. Mihacak. Theory and design of signal–adapted FIR paraunitary filter banks. *IEEE Trans. on Signal Processing*, 46:920–929, 1998.

S. T. Neely, S. J. Norton, M. P. Gorga, and W. Jesteadt. Latency of auditory brainstem responses and otoacustic emissions using tone-burst-stimuli. 83:652–656, 1988. J. Acoust. Soc. Am.

Ö. Özdamar and D. Alpsan. Neural network classifier for auditory evoked potentials. *Advances in Artificial Intelligence Research*, 2:165–175, 1992.

J. G. Peters. The ALGO–1: An automated infant hearing screener utilizing advanced evoked response technology. *Hear J.*, 89:335–353, 1986.

J. Pethe, R. Mühler, and H. von Specht. Amplitude modulation following response AMFR) in audiological diagnostics. *HNO*, 50:1045–1052, 2002.

P. K. Plinkert and W. Delb. Electronic data processing-assisted organization of interdisciplinary universal hearing screening in saarland. *HNO*, 49:888–894, 2001.

M. Popescu, S. Papadimitriou, D. Karamitsos, and A. Bezerianos. Adaptive denoising and multiscale detection of the v wave in brainstem auditory evoked responses. *Audiol. Neurootol.*, 4:38–50, 1999.

U. Richter and T. Fedtke. Reference zero for the calibration of audiometric equipment using clicks as test signals. 44:478–487, 2005. International Journal of Audiology.

M. Rosenblum, A. Pikovsky, and J. Kurths. Synchronization approach to analysis of biological system. *Fluctuations and Noise Letters*, 1:L53–L62, 2004.

M. Rosenblum, A. Pikovsky, J. Kurths, C. Schäfer, and P. A. Tass. Phase synchronization: from theory to data analysis. In A. J. Hoff, editor, *Handbook of Biological Physics*, pages 279–321, 2001.

A. P. Rudell. A fiber tract model of auditory brain-stem responses. *Electroencephalogr. Clin. Neurophysiol.*, 67:53–62, 1987.

R. Sanchez, A. Riquenes, and M. Perez-Abal. Automatic detection of auditory brainstem responses using feature vectors. *Int. J. Biomed. Comput.*, 39:287–297, 1995.

G. Shangkai and M. H. Loew. An autoregressive model of the BAEP signal for hearing threshold testing. *IEEE Trans Biomed Eng.*, 33:560–565, 1986.

M. Shensa. The discrete wavelet transform: Wedding the à trous and mallat algorithms. *IEEE Trans. Signal Processing*, 40:2464–2482, 1992.

M. M. Shoukri and C. A. Pause. *Statistical Methods for Health Sciences*. CRC Press LLC, Boca Raton, 1999.

E. P. Simoncelli, W. T. Freeman, E. H. Adelson, and D. J. Hegger. Shiftable multiscale transforms. *IEEE Trans. on Information Theory*, 38:587–608, 1992.

S. Sivalal. Screening for hearing loss in infants. Health Technology Assessment Report 2005, Malaysian Ministry of Health, 2005.

D. R. Stapells. Low-frequency hearing and the auditory brainstem response. *American Journal of Audiology*, 3:11–13, 1994.

D. R. Stapells. *A Sound Foundation Through Early Amplification: Frequency-specific evoked potential audiometry in infants.* R. C. Seewald. Phonak AG., Basel, 2000.

D. R. Stapells, R. Galambos, J. A. Costello, and S. Markeig. Inconsistency of auditory middle latency and steady-state responses in infants. *Electroencephalogr Clin Neurophysiol.*, 71:289–295, 1988.

J. Stevens, M. Foster, and S. Brennan. A comparison of ASSR and tone pip ABR with equivalent test parameters. NHS Conference, Como, Italy, 2004.

D. J. Strauss, W. Delb, R. D'Amelio, and P. Falkai. Neural synchronization stability in the tinnitus decompensation. In *Proceedings of the 2st Int. IEEE EMBS Conference on Neural Engineering*, pages 186–189, Arlington, VA, USA, 2005.

D. J. Strauss, W. Delb, R. D'Amelio, Y. F. Low, and P. Falkai. Objective quantification of the tinnitus decompensation by synchronization measures of auditory evoked single sweeps. *IEEE Trans Neural Syst Rehabil Eng.*, pages 74–81, 2008.

D. J. Strauss, W. Delb, and P. K. Plinkert. Analysis and detection of binaural inter-action in auditory brainstem responses by time–scale representations. *Computers in Biology and Medicine*, 24:461–477, 2004a.

D. J. Strauss, W. Delb, P. K. Plinkert, and H. Schmidt. Fast detection of wave V in ABRs using a smart single sweep analysis system. In *Conf Proc IEEE Eng Med Biol Soc*, pages 458–461, San Francisco, USA, 2004b.

D. J. Strauss and G. Steidl. Hybrid wavelet–support vector classification of waveforms. *Journal of Computational and Applied Mathematics*, 148:375–400, 2002.

D. J. Strauss, G. Steidl, and W. Delb. Feature extraction by shape–adapted local discriminant bases. *Signal Processing*, 83:359–376, 2003.

T. Strohmer. Rates of convergence for the approximation of dual shift-invariant systems in l2(z). *The Journal of Applied Fourier Analysis and Applications*, 5, 1999.

E. Stürzebecher, H. Wagner, M. Cebulla, and H.-J. Gerhardt. Timesaving frequency–specific threshold assessment in children using the bera notched–noise technique. In H. E. S. Hochmair-Desoyer, I. J., editor, *Advances in Cochlear Implants*, pages 89–92, Wien, Austria, 1994.

D. M. J. Tax and R. P. W. Duin. Data domain description using support vectors. In *Proceedings of European Symposium on Artificial Neural Networks '99*, Brugge, 1999.

P. P. Vaidyanathan. *Multirate Systems and Filter Banks*. Prentice Hall, Englewood Cliffs, NJ, 1993.

P. P. Vaidyanathan and P. Q. Hoang. Lattice structures for optimal design and robust implementation of two-channel perfect reconstruction qmf filter banks. *IEEE Trans. Acoust. Speech, and Signal Proc.*, 36:81–94, 1988.

E. Vannier, O. Adam, and J. F. Matsch. Objective detection of brainstem auditory evoked potentials with a priori information from higher presentation levels. *Artificial Intelligence in Medicine*, 25:283–301, 2002.

V. Vapnik. *The Nature of Statistical Learning Theory*. Springer, NY, 1995.

M. Vetterli and J. Kovačević. *Wavelets and Subband Coding*. Prentice-Hall, Englewood Cliffs, NJ, 1995.

G. Wahba. Support vector machines, reproducing kernel hilbert spaces and the randomized GACV. In B. Schölkopf, C. Burges, and A. J. Smola, editors, *Advanced in Kernel Methods – Support Vector Learning*, pages 293–306, Cambridge, MA, 1999.

O. Wegner and T. Dau. Frequency specificity of chirp–evoked auditory brainstem responses. 111:1318–1329, 2002. J. Acoust. Soc. Am.

J. D. Wicke, W. R. Goff, J. D. Wallace, and T. Allison. On–line statistical detection of average evoked potentials: Application to evoked response audiometry. *Electroenceph. Clin. Neurophysiol.*, 44:328–343, 1978.

M. V. Wickerhauser. *Adapted Wavelet Analysis form Theory to Software*. A. K. Peters, Ltd., Wellesley, MA, 1994.

W. Woodworth, S. Reisman, and A. B. Fointaine. The detection of auditory evoked responses using a matched filter. *IEEE Trans Biomed Eng.*, 20:369–376, 1983.

C. Yoshinaga-Itano. Benefits of early intervention for children with hearing loss. *Otolaryngol. Clin. North Am.*, 32:1089–1102, 1999.

Publications and Acknowledgments

Original Journal Papers, JCR/Medline listed

F. I. Corona–Strauss, W. Delb, B. Schick, and D. J. Strauss. Phase Stability Analysis of Chirp Evoked Auditory Brainstem Responses by Gabor Frame Operators, *IEEE Trans. on Neural Systems & Rehabilitation Engineering*, Accepted, 2009.

Mai Mariam, W. Delb, **F. I. Corona–Strauss**, M. Bloching and D. J. Strauss. Comparing the habituation of late auditory evoked potentials to loud and soft sound, *Physiol. Measurement*, 30:141–153, 2009.

F. I. Corona–Strauss, D. J. Strauss, B. Schick , W. Delb. Notched–Noise Embedded Frequency Specific Chirps for Objective Audiometry Using Auditory Brainstem Responses, Submitted.

F. I. Corona–Strauss, W. Delb, and D. J. Strauss. A Kernel–Based Novelty Detection Scheme for the Ultra–Fast Detection of Chirp Evoked Auditory Brainstem Responses, Submitted.

Articles in Journals (in Spanish)

F. I. Corona, J. A. Martínez. Desarrollo de instrumentación y prácticas para los laboratorios de fisiología I, II, y III y equipos de Diagnóstico y Terapia. *Mexican Magazine of Biomedical Engineering SOMIB*, 23:39–47, 2002.

Original Papers in Proceedings, Medline listed

D. J. Strauss, **F. I. Corona–Strauss**, C. Bernarding, W. Reith, M. Latzel, and M. Froehlich. On the Cognitive Neurodynamics of Listening Effort: A Phase Clustering Analysis of Large–Scale Neural Correlates, *Conf Proc IEEE Eng Med Biol Soc.*, pp. 2009:2078–2081, 2009.

F. I. Corona–Strauss, D. J. Strauss, B. Schick, and W. Delb. A Series of Notched–Noise Embedded Chirps for Objective Frequency Specific Hearing Examinations, *Conf Proc IEEE Eng Med Biol Soc.*, pp. 2009:2074–2077, 2009.

D. J. Strauss, **F. I. Corona–Strauss** and M. Froehlich. Objective Estimation of the Listening Effort: Towards a Neuropsychological and Neurophysical Model, *Conf Proc IEEE Eng Med Biol Soc.*, pp. 2008:1777–1780, 2008.

F. I. Corona–Strauss, W. Delb, M. Bloching and D. J. Strauss. On the Single Sweep Processing of Auditory Brainstem Responses: Click vs. Chirp Stimulations and Active vs. Passive Electrodes, *Conf Proc IEEE Eng Med Biol Soc.*, pp. 2008:4166–4169, 2008.

M. Busse, Y. F. Low, **F. I. Corona–Strauss**, W. Delb and D. J. Strauss. Neurofeedback by Neural Correlates of Auditory Selective Attention as Possible Application for Tinnitus Therapies, *Conf Proc IEEE Eng Med Biol Soc.*, pp. 2008:5136–5139, 2008.

Y. F. Low, C. Trenado, W. Delb, **F. I. Corona–Strauss** and D. J. Strauss. The Role of Attention in the Tinnitus Decompensation: Reinforcement of a Large–Scale Neural Decompensation Measure, *Conf Proc IEEE Eng Med Biol Soc.*, pp. 2007:2485–2488, 2007.

F. I. Corona–Strauss, W. Delb, M. Bloching, and D. J. Strauss. Ultra Fast Quantification of Hearing Loss by Neural Synchronization Stabilities of Auditory Evoked Brainstem Activity, *Conf Proc IEEE Eng Med Biol Soc.*, pp. 2007:2476–2479, 2007.

D. J. Hecker, W. Delb, **F. I. Corona**, and D. J. Strauss. Possible Macroscopic Indicators of Neural Maturation in Subcortical Auditory Pathways in School-Age Children, *Conf Proc IEEE Eng Med Biol Soc.*, pp. 2006:1173–1176, 2006.

C. Escobedo, F. Tovar, A. Vilá, J. Garc*í*a, B. Suárez, **F. I. Corona**, E. Sacristán. Hydrodynamic Effects of the Partial Opening of a Trileaflet Valve, *Conf Proc IEEE Eng Med Biol Soc.*, pp. 2006:2896–2899, 2006.

F. Tovar, C. Escobedo, G. Rodr*í*guez, J. Garc*í*a, A. Vilá, **F. I. Corona**, E. Sacristán. Structural Performance and Hydrodynamic Resistance of a New Silicone Auricular Cannula Tip, *Conf Proc IEEE Eng Med Biol Soc.*, pp. 2006:5396–5399, 2006.

F. I. Corona, R. Barragán, M. Calderón, H. Mart*í*nez, O. Infante, J. Molina, M. Lesprón, A. Hernández, C. Escobedo, J. Catrip, A. Gorzelewski, C. Tena, V. Graullera, E. Sacristán. Hemodynamic Performance In–Vivo of a new Ventricular Assist Device, *Conf Proc IEEE Eng Med Biol Soc.*, pp. 2005:394–397, 2005.

C. Escobedo, F. Tovar, B. Suárez, A. Hernández–God*í*nez, **F. I. Corona**, E. Sacristán. Experimental and Computer–Based Performance Analysis of Two Elastomer VAD Valve Designs, *Conf Proc IEEE Eng Med Biol Soc.*, pp. 2005:398–401, 2005.

E. Sacristán, **F. I. Corona**, B. Suárez, G. Rodríguez, B. Dueñas, A. Gorzelewski, M. Calderón. Development of a Universal Second Generation Pneumatic Ventricular Assist Device, *Conf Proc IEEE Eng Med Biol Soc.*, pp. 2003:427–430, 2003.

Conference Papers, Peer–Review, not in Medline

F. I. Corona–Strauss, W. Delb, B. Schick, S. Hussain and D. J. Strauss. Gabor Frame Phase Stability Analysis of Chirp Evoked Auditory Brainstem Responses, *In Proceeding of the 4th International IEEE EMBS Conference on Neural Engineering*, Antalya, Turkey, 2009, pp. 730–733.

D. J. Strauss, **F. I. Corona–Strauss**, M. Latzel and M. Fröhlich. On the Feasibility of Objective Listening Effort Estimations by Electroencephalographic Correlates of Corticofugal Modulations, *In Proceeding of the 4th International IEEE EMBS Conference on Neural Engineering*, Antalya, Turkey, 2009, pp. 34–37.

M. Mariam, W. Delb, **F. I. Corona–Strauss**, M. Bloching, and D J. Strauss. Extraction of Habituation Correlates in Single Sweep Sequences of Late Auditory Evoked Potentials using Time–scale Coherence: Objective Detection of Uncomfortable Loudness Level, *Biomed*, Innsbruck, Austria, 2008, pp. 601–605.

I. Mustaffa, **F. I. Corona–Strauss**, C. Trenado and D. J. Strauss. Nonlinear Diffusion Filtering of Single–Trial Matrix Representations of Auditory Brainstem Responses, *IFMBE Proceedings*, Antwerp, Belgium, 2008, pp. 429–432.

F. I. Corona–Strauss, W. Delb, M. Bloching, Sh. Hussain, and D. J. Strauss. The Johor Screening Scheme: Is an Area–Wide Newborn Hearing Screening Possible in Malaysia?, *In Proceedings of 3th International Conference of the IEEE IIHMSP*, Kaohsiung City, Taiwan, 2007, pp. 213–216.

Y. F. Low, **F. I. Corona–Strauss**, P. Adam, W. Delb, and D. J. Strauss. Extraction of Auditory Attention Correlates in Single Sweeps of Cortical Potentials by Maximum Entropy Paradigms and its Application, *In Proceeding of the 3rd International IEEE EMBS Conference on Neural Engineering*, Kohala Coast, HI, USA, 2007, pp. 469–472.

F. I. Corona–Strauss, D. J. Hecker, W. Delb, and D. J. Strauss. Ultra–Fast Detection of Hearing Thresholds by Single Sweeps of Auditory Brainstem Responses: A New Novelty Detection Paradigm, *In Proceeding of the 3rd International IEEE EMBS Conference on Neural Engineering*, Kohala Coast, HI, USA, 2007, pp. 638–641.

Published Conference Abstracts (Selection)

Note: *The independently published abstracts of the full proceedings papers cited before are not listed here again.*

F. I. Corona–Strauss, W. Delb, B. Schick and D. J. Strauss. Phase Stability Analysis of Chirp Evoked Auditory Brainstem Responses by Gabor Frame Operators, *80 Jahresversammlung der Deutschen Gesellschaft für HNO–Heilkunde, Kopf- und Hals-Chirurgie*, Rostock, Germany, 2009, pp.199.

F. I. Corona–Strauss, W. Delb, D. J. Strauss, and M. Bloching. Large Scale Neural Maturation Indicators in Subcortical Auditory Pathways in School–Age Children. *79. Jahresversammlung der Deutschen Gesellschaft für HNO–Heilkunde, Kopf- und Hals-Chirurgie*, Bonn, Germany, 2008, pp. 117.

M. Busse, Y. F. Low, **F. I. Corona–Strauss** and D. J. Strauss. Future for Tinnitus Therapies: Neurofeedback by Neural Correlates of Auditory Selective Attention, *X. International Conference in Cognitive Neuroscience (ICON X)*, Bodrum, Turkey, 2008, pp.394.

W. Delb W., **F. I. Corona–Strauss**, Y. F. Low and D. J. Strauss. ERP alterations related to tinnitus distress and attention, *9th International Tinnitus Seminars.* Gothenburg, Sweden, 2008, pp.30.

F. I. Corona–Strauss, W. Delb, M. Bloching, and D. J. Strauss. Fast detection of ABR–responses using neural synchronization stability and single sweep analysis, *78. Jahresversammlung der Deutschen Gesellschaft für HNO–Heilkunde, Kopf- und Hals-Chirurgie*, Heidelberg, Germany, 2007, pp.143.

W. Delb, Y. F. Low, **F. I. Corona–Strauss**, and D. J. Strauss. Auditory attention and tinnitus: the objective determination of tinnitus decompensation, *78. Jahresversammlung der Deutschen Gesellschaft für HNO–Heilkunde, Kopf- und Hals-Chirurgie*, Heidelberg, Germany, 2007, pp.109.

F. I. Corona, R. Barragán, M. Calderón, H. Martínez, O. Infante, J. Molina, M. Lesprón, A. Hernández, J. Catrip, A. Gorzelewski, C. Tena, V. Graullera, E. Sacristán. Desempeño Hemodinámico In vivo de un nuevo Dispotitivo de Asistencia Ventricular. *I Latin–American Congress of Cardiovascular and Thoracic surgery and XV Nacional Congress of Cardiac Surgery.* Mexico City, Mexico, 2006. in Spanish.

F. I. Corona, R. Barragán, M. Calderón, H. Martínez, O. Infante, J. Molina, M. Lesprón, A. Hernández, C. Escobedo, J. Catrip, A. Gorzelewski, C. Tena, V. Graullera, E. Sacristán. Desempeño Hemodinámico In Vivo de un nuevo Dispositivo de Asistencia Ventricular. *XIV National Cardiology Congress, and XX Interamerican Cardiology Congress.* Cancún, Mexico, 2006. in Spanish.

E. Sacristán, **F. I. Corona**, B. Suárez, G. Rodríguez, B. Dueñas, A. Gorzelewski, M. Calderón. Development of a Universal Second Generation Ventricular Pneumatic Assist Device and Drive Unit. *22nd Annual Symposium: Clinical Update in Anesthesiology.* Acapulco, Mexico, 2004.

Acknowledgments

First, I would like to express my gratitude to my supervisor PD Dr. med. Wolfgang Delb for his guidance, and the invaluable discussions and ideas during the entire process of this PhD project. Also, I wish to thank Prof. Dr. med. Bernhard Schick and Prof. Dr. med. Marc Bloching for giving me the opportunity to do this work at the Center for Research in Medical Communication Disorders.

I want to express my appreciation to my colleagues from the CDB–Unit, and the students of Saarland University of Applied Sciences (HTW) and Saarland University Hospital who were subjects once, or more times for the different paradigms tested during this project, particularly Lars Haab, Michael Busse, Yin Fen Low and Carlos Trenado. A special thanks to Andrea Rheinschmitt, Mrs. Roswitha Heinrich, Kevin Kern, and Vladislav Royter for their help with the logistics, and during the data acquisition process.

I would like to acknowledge all my teachers and professor along my entire student life, from the very beginning to the present stage. And I want to express my gratitude in particular to Dr. Emilio Sacristán R., and Jorge A. Martínez A., M. Sc. for their support during my first years as biomedical engineer, as well as for their advice and knowledge that they transferred me.

I also want to thank my parents in law, Gitta and Josef Strauss, and my German aunts –Erika, Gerda, Inge and Irene, for their warm welcome and for making me feel at home. To my brother, the family Chávez Barajas, my grandparents, and my Mexican and German friends: thank you for making everyday easier and funny!, and more important for still being in touch despite the distance.

And at last but not least, I thank my parents, Alfonso and Araceli, and my husband Daniel J. Strauss, for their encouragement, unconditional love and support at every second.

Curriculum Vitae

Personal Data

Name:	Farah Irene Corona–Strauss,
	(maiden name Corona Chávez)
Date of Birth:	14th. December 1977
Place of Birth:	Mexico City
Nationality:	Mexican
Marital Status:	Married

Education and Industry

1996–2001   Bachelor studies on Biomedical Engineering, degree conferred due to academic excellence, Universidad Iberoamericana, Mexico City, Mexico. Professional official licence number: 5714860.

2000–2001   Organization of the Council of Accreditation for the Education in Engineering (CACEI), Universidad Iberoamericana, Mexico City, Mexico.

2002–2003   Design Engineer, Innovamédica S.A. de C.V., Mexico City, Mexico.

2002–2006   Lecturer. Subjects: Hands on Sessions on Medical Instrumentation, and Electrodes and Transducers, Universidad Iberoamericana, Mexico City, Mexico.

2003–2006   Master of Science in Biomedical Engineering, Universidad Autónoma Metropolitana, Mexico City, Mexico. Professional official licence number: 3533706.

2004–2006	Head of Biomedical Engineering Department, Innovamédica S.A. de C.V., Mexico City, Mexico.
2006–2009	Researcher, European Center for Research in Medical Communication Disorders, Department of Otorhinolaryngology, Saarland University Hospital, Homburg, Germany.
2006–	Lecturer. Subjects: Biomaterials, Auditory Processing and Perception, Saarland University of Applied Sciences, Saarbruecken, Germany.
2009–	Chief Technical Officer of the Neural Engineering Lab., Computational Diagnostics & Biocybernetics Unit, Saarland University Hospital and Saarland University of Applied Sciences, Homburg/Saarbruecken, Germany.

Other Activities

Invited talks

- The Johor Newborn Hearing Screening Scheme, University Technology Malaysia, March 2007, Johor Bahru, Malaysia. (together with PD Dr. med. W. Delb)

- Hemodynamic Performance In Vivo of a new Ventricular Assist Device (In Spanish: Desempeño Hemodinámico In Vivo de un Nuevo Dispositivo de Asistencia Ventricular), Instrumentation Department of the National Institute of Cardiology Ignacio Chávez (INCICh), May 2006, Mexico City, Mexico.

- Technological Innovation in Mexico: Artificial Ventricle (In Spanish: Innovación Tecnológica en México: Ventrículo Artificial), within the framework of the 3rd Congress of Engineering, Universidad Iberoamericana, March 2004, Mexico City, Mexico.

Courses

- Thoratec Training Topics, Venue: Vitalmex International, 15–19 March 2004, Mexico City, Mexico.

- Cardiac failure: The state–of–the–art (In Spanish: Falla Cardiaca– El Estado del Arte), Venue: Hospital Angeles de las Lomas, 27–28 of March 2004, Mexico City, Mexico.

- Introduction to Biomaterials (In Spanish: Introducción a los Biomateriales), Venue: Center of Scientific Research of Yucatan (CICY), 21–23 October 2003, Merida, Mexico.

- Ventricular Support 2003: The state–of–the–art (In Spanish: Soporte Ventricular 2003: El Estado del Arte), Venue: Hospital Angeles de las Lomas, 14–15 March 2003, Mexico City.

Academic Supervision

Hochschule für Technik und Wirtschaft des Saarlandes, Saarbruecken, Germany

- Bachelor BE⋆: Corinna Bernarding. Development of Experimental Paradigm for the Listening Effort Estimation, 2008.

- Bachelor BE⋆: Mathias Vukelic. Otoacustic Emissions Prototype developed under MATLAB, 2008.

- Bachelor BE⋆: Andreas Bohr. High–Speed C++ Interface for Biosignal Amplifiers, since 2008.

- Master BE⋆: Dominik Wagner. Optimal Cochlear Stimulation using Evolutionary Neurofeedback Programming, 2009.

- Master BE⋆: Michael Busse. Neurofeedback for Tinnitus Therapies, 2007.

Instituto Politécnico Nacional, Mexico City, Mexico

- Bachelor BE⋆: Fernando Fabian Hernández Hernández. Estancia en Innovamédica, papel del Ingenierio Biomédico en Investigación y Desarrollo de equipo Médico, 2005.

⋆BE: Biomedical Engineering.

Awards

Recognition for the best Biomedical Engineering score. Universidad Iberoamericana, Mexico City, Mexico, 2001.

Memberships

IEEE (Institute of Electrical and Electronic Engineers)
EMBS (Engineering in Medicine and Biology Society)
SOMIB (Sociedad Mexicana de Ingeniería Biomédica (Mexican Society of Biomedical Engineering))

Languages

Spanish: mother tongue
English: fluent
German: beginner level